

1 Phenomenology of summer ozone episodes over the Madrid 2 Metropolitan Area, central Spain

3 Xavier Querol¹, Andrés Alastuey¹, Gotzon Gangoiti², Noemí Perez¹, Hong K. Lee³, Heeram R.
4 Eun³, Yonghee Park³, Enrique Mantilla⁴, Miguel Escudero⁵, Gloria Titos¹, Lucio Alonso², Brice
5 Temime-Roussel⁶, Nicolas Marchand⁶, Juan R. Moreta, M. Arantxa Revuelta⁷, Pedro Salvador⁸,
6 Begoña Artíñano⁸, Saúl García dos Santos⁹, Mónica Anguas¹⁰, Alberto Notario¹¹, Alfonso Saiz-
7 Lopez¹⁰, Roy M. Harrison¹², Millán Millán⁴, Kang-Ho Ahn³

8
9 ¹Institute of Environmental Assessment and Water Research (IDAEA-CSIC), C/Jordi Girona 18-26, Barcelona, 08034
10 Spain

11 ²Escuela Técnica Superior Ingeniería de Bilbao, Departamento Ingeniería Química y del Medio Ambiente,
12 Universidad del País Vasco UPV/EHU, Urkixo Zumarkalea, S/N, Bilbao, 48013 Spain

13 ³Department of Mechanical Engineering, Hanyang University, Ansan 425-791, Republic of Korea

14 ⁴Centro de Estudios Ambientales del Mediterráneo, CEAM, Unidad Asociada al CSIC, Parque Tecnológico C/ Charles
15 R. Darwin, 14 Paterna, Valencia, 46980 Spain

16 ⁵ Centro Universitario de la Defensa de Zaragoza, Academia General Militar, Ctra. de Huesca s/n, Zaragoza, 50090
17 Spain

18 ⁶Aix Marseille Univ, CNRS, LCE, Marseille, France

19 ⁷Agencia Estatal de Meteorología, AEMET, C/ Leonardo Prieto Castro, 8, Madrid, 28071 Spain

20 ⁸Department of Environment, CIEMAT, Joint Research Unit Atmospheric Pollution CIEMAT-CSIC, c/ Avenida
21 Complutense 40, Madrid, 28040 Spain

22 ⁹Centro Nacional de Sanidad Ambiental. Instituto de Salud Carlos III (ISCIII), Ctr Majadahonda a Pozuelo km 2,
23 Majadahonda (Madrid), 28222 Spain

24 ¹⁰Department of Atmospheric Chemistry and Climate, Institute of Physical Chemistry Rocasolano, CSIC, Madrid,
25 28006 Spain

26 ¹¹University of Castilla-La Mancha, Physical Chemistry Department, Faculty of Chemical Science and Technologies,
27 Ciudad Real, Spain.

28 ¹²National Centre for Atmospheric Science, University of Birmingham, B15 2TT United Kingdom. †Also at:
29 Department of Environmental Sciences/Centre for Excellence in Environmental Studies, King Abdulaziz University,
30 Jeddah, Saudi Arabia

31

32 Abstract

33 Various studies have reported that photochemical nucleation of new ultrafine particles (UFP)
34 in urban environments within high insolation regions occurs simultaneously with high ground
35 ozone (O₃) levels. In this work, we evaluate the atmospheric dynamics leading to summer O₃
36 episodes in the Madrid Air Basin (Central Iberia) by means of measuring a 3D distribution of
37 concentrations for both pollutants. To this end, we obtained vertical profiles (up to 1200 m
38 above ground level) using tethered balloons and miniaturised instrumentation at a suburban
39 site located to the SW of the Madrid Metropolitan Area (MMA), the Majadahonda site (MJDH),
40 in July 2016. Simultaneously, measurements of an extensive number of air quality and
41 meteorological parameters were carried out at 3 supersites across the MMA. Furthermore,
42 data from O₃-soundings and daily radio-soundings were also used to interpret atmospheric
43 dynamics.

44 The results demonstrate the concatenation of venting and accumulation episodes, with
45 relative lows (venting) and peaks (accumulation) in O₃ surface levels. Regardless of the episode
46 type, fumigation of high-altitude O₃ (arising from a variety of origins) contributes the major
47 proportion of surface O₃ concentrations. Accumulation episodes are characterised by a
48 relatively thinner planetary boundary layer (planetary boundary level (PBL) < 1500 m at
49 midday, lower in altitude than the orographic features), light synoptic winds, and the

50 development of mountain breezes along the slopes of the Guadarrama Mountain Range
51 (located W and NW of MMA, with a maximum elevation of >2400 m above sea level). This
52 orographic-meteorological setting causes the vertical recirculation of air masses and
53 enrichment of O₃ in the lower tropospheric layers. When the highly polluted urban plume from
54 Madrid is affected by these dynamics, the highest O_x (O₃+NO₂) concentrations are recorded in
55 the MMA.

56 Vertical O₃ profiles during venting episodes, with strong synoptic winds and a deepening of the
57 planetary boundary layer, reaching >2000 m above sea level, were characterised by an upward
58 gradient in O₃ levels, whereas a reverse situation with O₃ concentration maxima at lower levels
59 was found during the accumulation episodes due to local/regional production. The two
60 contributions to O₃ surface levels (fumigation from high altitude strata and local/regional
61 production) require very different approaches for policy actions. In contrast to O₃ vertical top-
62 down transfer, UFP are formed in the lowest levels and are transferred upwards progressively
63 with the increase in the increase of the planetary boundary layer.

64

65 **Keywords:** Ozone, ultrafine particles, photochemical pollution, air quality, vertical profiles.

66

67

68 **1. Introduction**

69 The EU Directive 2008/50/EC on ambient air quality, amended by Directive 2015/1480/EC,
70 establishes the need to comply with air quality standards to protect citizens and ecosystems. If
71 these are not met, plans to improve air quality must be implemented by the national, regional,
72 and local administrations. Despite the considerable improvements in air quality during the last
73 decade, non-compliance with European air quality standards is still reported in most of
74 Europe. In particular, the limit values for nitrogen dioxide (NO₂), particulate matter (PM₁₀ and
75 PM_{2.5}) and the tropospheric ozone (O₃) target value are frequently exceeded (EEA, 2017).
76 Therefore, in 2013, the National Plan for Air Quality and Protection of the Atmosphere (Plan
77 AIRE), 2013-2016, was drawn up, and approved by the Spanish Council of Ministers'
78 Agreement of 12 April 2013.

79 The EEA (2017) recently reported that, in 2015, 80% of the urban EU-28 population was
80 exposed to PM_{2.5} levels exceeding the WHO guideline, and 90% to that of O₃.

81 Measures to effectively reduce NO₂ and primary PM pollution are relatively easy to identify
82 (such as abating industrial, shipping, and traffic emissions with catalytic converters for NO_x and
83 particulate controls for PM). However, defining policies for abating O₃, other photochemical
84 pollutants, and the secondary components of PM is much more complex.

85 Photochemical pollution is a subject of great environmental importance in Southern Europe
86 due to its climatic and geographical characteristics (Ochoa-Hueso, 2017). Products of this type
87 of pollution are many, the most noteworthy being tropospheric O₃, secondary PM (nitrate,
88 sulphate, and secondary organic compounds), and the generation of new ultra-fine particles
89 (UFPs) by nucleation (Gomez-Moreno et al., 2011; Brines et al., 2015). In summer, the Western

90 Mediterranean Basin (WMB), surrounded by high mountains, falls under the influence of the
91 semi-permanent Azores anticyclone. Clear skies prevail under a generalized level of subsidence
92 aloft, and meso-meteorological processes with marked diurnal cycles dominate. Re-circulation,
93 strong insolation, and stability in the upper layers favour the production/accumulation of O₃
94 (Millán et al., 1997, 2000, 2002; Kalabokas et al., 2008; Giannakopoulos et al., 2009; Velchev et
95 al., 2011; Sicard et al., 2013) and the emissions of biogenic volatile organic compounds
96 (BVOCs) (Giannakopoulos et al., 2009).

97 The abatement of tropospheric O₃ levels in this region is a difficult challenge due to its origin,
98 which may be local, regional, and/or transboundary (Millán et al., 2000; Millán, 2014; Lelieveld
99 et al., 2002; Kalabokas et al., 2008, 2013, 2015, 2017; Velchev et al., 2011; Sicard et al., 2013;
100 Zanis et al., 2014), the complexity of the meteorological scenarios leading to severe episodes
101 (Millán et al., 1997; Gangoiti et al., 2001; Dieguez et al., 2009, 2014; Kalabokas et al., 2017), as
102 well as the complexity of the non-linear chemical processes that drive its formation and sinks
103 (Monks et al., 2015, and references therein).

104 This complex context has led to a lack of 'sufficient' O₃ abatement in Spain (and Europe); while
105 for primary pollutants, such as SO₂ and CO, and the primary fractions of PM₁₀ and PM_{2.5}
106 improvement has been very evident (EEA, 2017). Thus, the latest air quality assessment for
107 Europe (EEA, 2017) shows that: i) there has been a tendency for the peak O₃ concentration
108 values (those exceeding the hourly information threshold of 180 µg/m³) to decrease in recent
109 years, although not enough to meet the WHO guidelines and EC standards; and ii) the problem
110 of O₃ episodes is more pronounced in the South than in Northern and Central Europe.
111 Likewise, O₃ levels are higher in rural than in urban areas, both due to i) the generation
112 process, which requires time since the emissions of urban, industrial and biogenic precursors
113 to the production of O₃; and ii) the consumption (NO titration) of O₃ that takes place in urban
114 areas.

115 Other studies, such as Sicard et al. (2013), Paoletti et al. (2014), Escudero et al. (2014),; Garcia
116 et al. (2014), Querol et al. (2014, 2016), and EMEP (2016), also evidenced that there is a
117 general tendency for O₃ to increase in urban areas, including at traffic sites, probably due to
118 the greater reduction of NO emissions relative to NO₂ and, therefore, a lower NO titration
119 effect. This trend in decreasing NO/NO₂ ratios from diesel vehicle emissions (the main source
120 of NO_x in urban Europe) has been widely reported (i.e., Carslaw et al., 2016). It has also been
121 found that regional background O₃ levels have remained constant over the last 15 years, while
122 acute episodes have been drastically reduced compared to the late 1990s, although these
123 markedly increase during heat waves, such as those in the summers of 2003 and 2015 (EEA,
124 2017; Diéguez et al., 2009, 2014; Querol et al., 2016).

125 A recent study (Saiz-Lopez et al., 2017) reported an increase of 30-40% in ambient air O₃ levels,
126 along with a decrease of 20-40% in NO₂, from 2007 to 2014 in Madrid, which may have led to
127 large concentration increases of up to 70% and 90% in OH and NO₃, respectively, thereby
128 changing the oxidative capacity of this urban atmosphere. We still do not know if this increase
129 is due to a decrease in the NO titration effect or to the fact that O₃ formation is dominated by
130 VOCs since the urban areas are characterized by 'VOC-limited' conditions, and a reduction in
131 NO_x emission might yield an increase in O₃ formation.

132 Intensive research on O₃ pollution has been carried out in the Mediterranean since the late
133 1980s and has been key in understanding the behaviour of this pollutant in Europe. It has also
134 been used to establish current European air quality standards (Millán et al., 1991, 1996a,
135 1996b, 1996c, 2000, 2002; Millán, 2002; Lelieveld 2002; EC, 2002, 2004; Millán and Sanz, 1999;
136 Mantilla et al., 1997; Salvador et al., 1997, 1999; Gangoiti et al., 2001; Stein et al., 2004, 2005;
137 Chevalier et al., 2007; Kalabokas et al., 2008, 2015, 2017; Castell et al., 2008a, 2008b, 2012;
138 Kulkarni et al., 2011; Velchev et al., 2011; Doval et al., 2012; Sicard et al., 2013; Millán et al.,
139 2014; Escudero et al., 2014; Zanis et al., 2014; Sicard et al., 2017, among others). The EEA
140 (2017) reports a clear increase in exceedances of the human protection 8-h O₃ target value in
141 Southern and Central Europe, which are higher in the Italian Po Valley and Spain, and relatively
142 lower in Portugal and the Eastern Mediterranean.

143 Focusing on the study area, Diéguez et al. (2009, 2014) describe in detail the temporal and
144 spatial variation of O₃ levels in Spain. These studies highlight the low inter-annual variability in
145 regional background stations, as well as the existence of specific areas, such as the Madrid air
146 basin (MAB), Northern valleys influenced by the Barcelona urban plume, Puertollano basin,
147 and the interior of the Valencian region, where very high O₃ episodes are relatively frequent,
148 and point to urban and industrial hot spots as relevant sources of precursors. Recently, Querol
149 et al. (2016) evidenced that the highest O₃ episodes, with hourly exceedances of the
150 information threshold for informing the population (180 µg/m³) during 2000-2015, occurred
151 mostly around these densely populated or industrialised areas.

152 Querol et al. (2017) report that the high-O₃ plume transported from the metropolitan area of
153 Barcelona contributed decisively to the frequent exceedances of the information threshold in
154 the northern areas of Barcelona during the acute O₃ episodes in July 2015. They also
155 demonstrate that the associated meteorology was very complex, similar to the vertical
156 recirculation of air masses scenarios reported by Gangoiti et al. (2001), Millán (2014) and
157 Diéguez et al. (2014) for other regions of the Western Mediterranean. Regional transport of O₃
158 is also very relevant, as well as acute O₃ episodes, which exceeded the information threshold
159 and were caused largely by regional transport (with large a contribution also from local
160 formation recirculated during prior days, on top of which an additional smaller local 'fresh'
161 contribution was added). It is also shown that the vast majority of these exceedances are
162 recorded in July.

163 In the Eastern Mediterranean, the regional background O₃ levels in the free troposphere and
164 the boundary layer during summer might regularly exceed 60 ppb, and fumigation of these
165 upper air masses contributes, on average, to the greatest part of the surface O₃ levels
166 measured in Greece (Kalabokas et al., 2000; Kourtidis et al., 2002; Kouvarakis et al., 2002;
167 Lelieveld et al., 2002; Kalabokas and Repapis, 2004; Gerasopoulos et al., 2005). Furthermore, a
168 number of studies report contributions from the stratosphere to the surface O₃ concentrations
169 during specific meteorological scenarios in the same region (Kalabokas et al., 2013, 2015;
170 Zanis et al., 2014; Parrish et al., 2012; Lefohn et al., 2012; Akritidis et al., 2016, among
171 others). In addition, recent research shows that, during springtime O₃ episodes (April – May)
172 over the WMB, similar synoptic meteorological patterns might also occur, and that these are
173 linked with regional episodes, mainly induced by large-scale tropospheric O₃ subsidence,
174 influencing the boundary layer as well as the ground surface O₃ concentrations (Kalabokas et

175 al., 2017). However, the most intense episodes in the WMB occur in June-July, according to the
176 statistics for the 2000-2015 period in Spain presented by Querol et al. (2016).

177 In addition to primary emissions, nucleation or new particle formation (NPF) processes give
178 rise to relevant contributions to the urban ambient air UFP concentrations, mostly during
179 photochemical pollution episodes in spring and summer (Brines et al., 2015, and references
180 therein). Ambient conditions favouring urban NPF are high insolation, low relative humidity,
181 available SO₂ and VOCs, as well as a low condensation sink potential (i.e., a relatively clean
182 atmosphere with low surface aerosol concentrations) (Kulmala et al., 2000, 2004; Kulmala and
183 Kerminen, 2008; Sipilä, et al., 2010; Salma et al., 2016).

184 In this study, we evaluate the temporal and spatial variability of O₃ and UFP in the MAB (04-
185 20/07/2016), to investigate the causes of acute summer episodes of both pollutants and
186 possible inter-relationships. In a subsequent twin article, we will focus on the phenomenology
187 of UFP nucleation episodes linked with these photochemical events. Data on UFPs are
188 included in this paper only where they assist in interpreting the behaviour of O₃.

189

190 **2. Methodology**

191 **2.1. The study area**

192 The MAB and the Madrid Metropolitan Area (MMA) are located in the central plain, or Meseta,
193 of the Iberian Peninsula at around 700 m above sea level (m a.s.l.). Regarding the topographic
194 features, the Guadarrama range, which runs in the NE-SW direction, reaches heights of up to
195 2400 m a.s.l. and is located 40 km north from the MMA. To the S, are the Toledo Mountains
196 which run from E to W (Figure 1). Lower mountains, located to the NE and E, are part of the
197 Iberian range. Consequently, the Madrid plain shows a NE-SW channelling of winds, forced by
198 the main mountain ranges, following the basin of the Tagus River and its tributaries. In
199 particular, the MMA is located to the NE of the river basin and on its E side.

200 Climatologically, the area is characterised by continental conditions with hot summers and
201 cold winters, with both seasons typically being dry. Mean annual precipitation of
202 approximately 400 mm is mainly concentrated in the autumn and spring. The MMA is one of
203 the most densely populated regions in Spain, with more than 5 million inhabitants, including
204 Madrid City and surrounding towns. According to Salvador et al. (2015), the main
205 anthropogenic emissions are dominated by road traffic and residential heating (in winter), with
206 minor contributions from industry and a large airport.

207 Figure 2 shows the time series of the recorded meteorology, measured at a surface station
208 representative of the conditions in the MMA during the field campaign of July 2016 (El Retiro,
209 in central Madrid). In order to put the field campaign into the context of the more general
210 meteorological situation, the time series is extended backwards to the end of June and
211 forward to the end of July 2016. Figure 2 also shows the corresponding time series for O₃, NO₂,
212 and O_x concentrations in the MMA, demonstrating the occurrence of well-marked peaks
213 alternating with relatively low O₃ and O_x concentrations periods. The intensive field campaign
214 (11-14/07/2016, marked with a green frame) coincides with a low O₃ interval preceding a
215 higher O₃ period in the last two days. Red and blue frames in Figure 2 show days in which high-

216 resolution O₃ free soundings were performed (red and blue indicating intervals within high and
217 low O₃, respectively).

218

219 **2.2. Monitoring sites and instrumentation**

220 To characterise acute summer episodes of O₃ and UFP and to investigate their possible
221 relationships, we devised an intensive field campaign in the MMA. Three measurement
222 supersites in and around Madrid, following a WNW direction, according the previously
223 described dynamics, were deployed in an area where the highest levels of O₃ (with hourly
224 maxima sporadically exceeding 180 µg/m³) are usually recorded (Reche et al., 2018, submitted)
225 inside the MAB (Figure 1). Table 1 shows the equipment available at the three following
226 supersites:

- 227 • Madrid-CSIC, located at the Spanish National Research Council headquarters. This site is
228 located in central Madrid on the sixth floor of the building of the Instituto de Ciencias
229 Agrarias.
- 230 • CIEMAT, located at the Centro de Investigaciones Energéticas Medioambientales y
231 Tecnológicas headquarters, 4 km in a WNW direction from the CSIC site in a suburban
232 area.
- 233 • MJDH-ISCI, located in the Instituto de Salud Carlos III in Majadahonda, 15 km in a NW
234 direction from the CSIC site.

235 At MJDH-ISCI, a PTR-ToF-MS (Proton Transfer Reaction-Time of Fly-Mass Spectrometry) was
236 deployed from 04 to 19/07/2017 and provides insights into the O₃ Formation Potential (OFP)
237 of the VOC mixture over the MMA area. The operation procedure of the PTR-ToF-MS and OFP
238 calculation are detailed in Table S1 and Figure S1.

239 Furthermore, from 11 to 14/07/2016, 28 profiles of pollutant and meteorological parameters
240 up to 1200 m above ground level (m a.g.l.) were obtained using tethered balloons and a fast
241 winch system (Figure S1, Tables 2). The instrumentation attached to the balloons is
242 summarised in Table 1. The profiles were performed at the Majadahonda Rugby Course
243 (MJDH-RC Figure 1). The balloons were equipped with a Global Position System (GPS) and a set
244 of instruments (Figure S3), including:

- 245 • A miniaturized CPC (Condensation Particle Counter built by Hanyang University, Hy-CPC)
246 was used to measure the number concentration of particles larger than 3 nm (PN₃) with a
247 time resolution of 1 s and a flow rate of 0.125 L/min, using butanol as a working fluid (Lee
248 et al., 2014). Previous inter-comparison studies with conventional CPCs have yielded very
249 good results (with r² reaching 0.65-0.98 and slopes 0.87-1.23, Minguillón et al., 2015). In
250 this work, we will use the terms UFP and PN₃ as equivalents, but we measure
251 concentrations between 3 and 1000 nm strictly while UFP is <100 nm. However, 80% of
252 the total particle concentration falls in the range of UFPs.
- 253 • An O₃ monitor (PO3M, 2B Technologies) was used to determine O₃ concentrations. It was
254 calibrated against an ultraviolet spectrometry reference analyser showing good
255 agreement (n=34; PO3MO₃=1.1058*RefO₃+4.41, R²=0.93). Concentrations (on 10 s basis)

256 are reported in standard conditions (20 °C and 101.3 kPa) and corrected for the reference
257 method.

258 In addition to the above instrumentation, we obtained the following additional meteorological
259 and air quality data:

260 • Meteorological data from the CIEMAT meteorological tower (four instrumented levels
261 between surface and 54 m a.g.l.), as well as from several AEMET (Spanish Met Office)
262 standard meteorological stations spread out across the basin: Madrid Airport (40.46°N,
263 3.56°W, 609 m a.s.l), Colmenar Viejo (40.69°N, 3.76°W, 994 m a.s.l), and El Retiro (in
264 Madrid, 40.40°N, 3.67°W, 667 m a.s.l).

265 • Hourly data for air pollutants (NO, NO₂, SO₂, O₃, PM₁₀, and PM_{2.5}) supplied by the air
266 quality networks of the city of Madrid, the Regional Governments of Madrid, Castilla La
267 Mancha, Castilla y León, and the European Monitoring and Evaluation Programme (EMEP)
268 monitoring network, all of them supplied by the National Air Quality Database of the
269 Ministry of the Environment of Spain (MAPAMA).

270 • High-resolution O₃-sounding data performed by AEMET at midday each Wednesday at
271 Madrid Airport.

272 • High-resolution meteorological sounding data obtained each day at 00:00 and 12:00 h
273 local time by AEMET, also at Madrid Airport. They were used to estimate the height of the
274 planetary boundary layer (PBL) at 12:00 UTC by means of the simple parcel method
275 (Pandolfi et al., 2014).

276 Hourly averaged wind components were calculated and used in polar plots with hourly PM₁,
277 PM_{2.5}, NO₂, O₃, O_x (O₃+NO₂), BC, and UFP concentrations by means of the OpenAir R package
278 (Carslaw and Ropkins, 2012).

279

280 **3. Results**

281 **3.1. Meteorological context**

282 The AEMET O₃-soundings are represented in Figure 3, where it is evident that the low/high O₃
283 periods coincide with the 500 hPa gph passage of, respectively, upper level troughs/ridges
284 over the area, associated with cold/warm deep advection of air masses. Cold advectons have
285 usually an Atlantic origin.

286 The local meteorology during the field campaign was characterized by a progressive drop in
287 temperature (T) (-4°C in the maximal daily T) and an increase in the early morning relative
288 humidity (RH) (+20%), with insolation remaining constant (maxima of 900-950 W/m²) (Figure
289 4). During the nocturnal and early morning conditions of the first half of the field campaign
290 (11-12/07/2016), relatively weak northerly winds prevailed at the main meteorological surface
291 stations inside the basin, including CIEMAT in Figure 4, and Retiro and Colmenar in Figure S4.
292 This is probably related to drainage (katabatic) conditions inside the MAB, with a progressive
293 turn to a more synoptic westerly component in the central period of the day, consistent with a
294 convective coupling with the more intense upper level wind. This coupling is also accompanied
295 by an important increase in the wind speed at midday, up to 8 m/s (venting stage), that
296 renewed air masses in the whole basin.

297 During the second half of the campaign, intense and persistent north-easterly winds replaced
298 the westerlies from the evening of 12/07/2016 on, after the evolution of the upper level
299 trough. In contrast to the previous period, during 13-14/07/2016, night-time and early
300 morning conditions registered more intense NE winds (up to 10 m/s) than at midday, after a
301 decrease in intensity down to calm conditions (1 m/s) during the 12/07 morning, facilitating
302 both fumigation from upper levels and local O₃ photochemical production. A weak wind
303 veering to the south was also registered at the mentioned surface stations during the 13/07
304 afternoon, which lasted for only 3 hours, and which is more characteristic of an O₃ enrichment
305 episode, when the veering lasted longer (Plaza et al., 1997). A progressive decrease of the PBL
306 height (-600 m difference) is observed in the AEMET daily radio-soundings, in particular,
307 gradual decreases in the midday PBL height of 3400, 2200, 1900, and 1600 m a.s.l. from 11 to
308 14/07/2016 (Figure S5) were observed. This decrease is also observed in the 12 and
309 14/07/2017 UFP profiles (Figures 5 and 6 and S6-S8). As will be detailed later, these
310 meteorological patterns allowed O₃ and UFP to smoothly and progressively accumulate in the
311 basin (Figure 4) during the campaign.

312 In the vertical dimension, during both the high and low O₃ periods analysed here, all the
313 soundings show at midday two well-defined layers separated by a temperature inversion
314 marking the limit of the growing convection inside the PBL (Figure 3).

315 In high O₃ periods (6 and 27/07/2016), we found lower PBL heights (approximately 1300-1500
316 m a.s.l.), with weak winds from the E or NE (less than 4-5 m/s) or calm conditions. This is
317 consistent with the scheme proposed by Plaza et al. (1997), who also describe a rapid
318 evolution of the PBL height up to 2500-3000 m a.s.l. at 15:00 UTC during their field campaigns
319 in the area under “summer anticyclonic conditions.” They also describe a morning radiative
320 surface inversion at around 1000 m a.s.l., which was usually “destroyed 1 hour after dawn,”
321 containing NE winds associated with nocturnal drainage flows at lower levels (following the
322 slope of the MAB). In this context, residual layers containing pollutants processed during the
323 previous day(s) can develop above the stably stratified surface layer during night-time
324 conditions. These pollutants can be transported towards the S by weak north-easterly winds,
325 or remain stagnant under calm conditions, which leads to fumigation and mixing with fresh
326 pollutants emitted at the surface after the destabilization of the surface layer, as we evidenced
327 in our profiles. These residual layers are topped by the subsidence anticyclonic inversion
328 (1000-1500 m a.s.l.), according to Plaza et al. (1997).

329 Conversely, the soundings corresponding to low O₃ periods have in common more elevated
330 PBL heights (2000-2500 m a.s.l.), with more intense winds (above 6-7 m/s) that can blow from
331 different sectors: from the NE, on 13/07/2016 (with intense N-Westerlies blowing in the free
332 troposphere), or the S-SW, as observed on 29/06/2016 and 20/07/2016. The O₃-sounding on
333 13/07/2016, a unique day within the field campaign, presents the final stage of a low O₃
334 period, with winds in the free troposphere having a clear NW component while channelled
335 north-easterly winds dominate below 2000 m a.s.l. The AEMET free-sounding shows low O₃
336 surface concentrations (<45 ppb) and high levels (>70 ppb) in the middle troposphere (3000-
337 5000 m a.s.l.), associated with very low relative humidity and intense W to NW winds blowing
338 at that height, which will be discussed in Section 4. The decrease of surface temperature
339 observed in Figure 2 during the field campaign is also consistent with the cold advection
340 associated with the troughing in the 500 hPa heights (13/07/2016 in Figure 3).

341

342 **3.2. Surface O₃, O_x, and UFP during the field campaign**

343 As previously stated, the field campaign was characterised by atmospheric venting conditions
344 with the two last days marking a transitional period to a more stable anticyclonic episode of
345 increasing O₃. The lowering of the wind speed during diurnal periods, and other meteorological
346 features mentioned above, favoured the gradual accumulation of pollutants, as indicated by
347 the progressive increase of the O₃ maxima at MJDH-ISCI, where the O₃ maximum was reached
348 at 15:00 UTC on 13/07/2016 and at 17:00 UTC on 14/07/2016 (Figure 4). The typical
349 accumulation O₃ cycle for the zone was found only on 13 and 14/07/2016, with a maximum at
350 14:00 UTC on 13/07/2016 and at 16:00 UTC on 14/07/2016. The two previous days presented
351 a more irregular daily pattern, indicating unstable and atypical situations for July (perturbed
352 conditions with the prevalence of synoptic winds). Furthermore, these meteorological
353 conditions and the high insolation induced the concatenation of NPF episodes in the basin
354 (with low BC and very high UFP levels at the central hours of the day), such as the one on
355 13/07/2016 (Figure S9). Morning-midday UFP bursts were caused by nucleation and growth
356 episodes (we will focus on the phenomenology and the vertical occurrence of these
357 nucleation-growth events in the twin article).

358 From 11 to 12/07/2016 the highest concentrations of O₃ were recorded for W-SW and W
359 winds, and peak UFP (PN₃) concentrations were observed with W, SW, WNW, and NE winds.
360 However, on 13-14/07/2016, both O₃ and UFP concentrations maximized during calm and NE
361 winds (see polar plots from Figure S10). PM_{2.5} levels were independent of the UFP and O₃
362 variation, with concentrations increasing in calm situations in the first two days, and with less
363 pronounced variations as a function of the wind direction, but somewhat higher concentrations
364 with NE winds in the last two days (Figure S10).

365

366 **3.3. Vertical O₃ and UFP profiles during the field campaign**

367 As shown in Figure S2 and Table 2, the vertical profiles for 14/07/2016 were the most
368 complete of the campaign (wind speed was relatively low and this allowed extended
369 measurements throughout the day), and, for that reason, we begin with the description of this
370 day.

371 Figure 5 shows that there is a rapid growth of the PBL between 08:05 and 11:01 h UTC, as
372 deduced from the vertical profile of UFP (PN₃₋₃₀₀) concentrations. At the beginning of the
373 measurements, the upper limit of the PBL was above 1030 m a.s.l., and in 2 h 40 min it lifted
374 400 m (around 2.5 m/min). In this initial period, the vertical profile of O₃ was characterized by
375 a succession of strata of different concentrations, but a clear tendency to increase with height
376 (around 20 ppb of difference between surface level and 1950 m a.s.l. was observed). The
377 discontinuity of the PBL ceiling reflected in the UFP, T, and RH profiles did not seem to affect
378 the O₃ profile at all. In other words, we did not notice accumulation of O₃ layers in the top of
379 the PBL, but, instead, a general increasing trend towards the highest altitudes reached with
380 the tethered balloons.

381 Through the course of the day, the profile of concentrations of UFP and O₃ became
382 homogenous in the lowest 1200 m a.g.l. (this being the maximum height reached), and a

383 growth of O₃ concentrations at all altitudes was observed until 16:11 h UTC. This
384 homogenisation and growth of O₃ concentrations in the PBL, caused by intense mixing by
385 convection, resulted in an uneven increase through the day with an increase of 43 ppb at
386 surface and only 10 ppb at 1900 m a.s.l. (Figures 5 and S6).

387 Figure 6 shows the results from measurements taken at a fixed height (1400-1200 m a.s.l.)
388 made to capture the effect of the growth of the PBL on O₃ and UFP levels. We started at
389 approximately 700 m a.g.l. at 09:32 UTC with 60 ppb of O₃ and approximately 6000 #/cm³. At
390 10:25 UTC, the top of the PBL reached the balloon, as deduced from the sharp increase in UFP
391 concentrations (up to 20000 #/cm³). Meanwhile, O₃ concentrations experienced only a slight
392 decrease, suggesting that O₃ fluxes are top down and not bottom up, as recorded for UFP.
393 From 16:11 h UTC onwards, a reduction of O₃ levels at lower heights was observed (-50 ppb at
394 surface levels from 15:55 to 17:45 h UTC, while at 1900 m a.s.l. levels remained stable, Figures
395 5 and S6).

396 The soundings of 11 to 13/07/2016 again showed a vertical trend characterised by: i) higher O₃
397 concentrations at the highest sounding altitude in the early morning, ii) an increase in O₃
398 concentrations as the morning progressed (more pronounced at low altitudes), and iii)
399 homogenous O₃ concentration along the entire vertical profile, except in the surface layers,
400 where the deposition and titration markedly decreased O₃ levels reached at midday. Detailed
401 descriptions of these soundings (Figures S7 and S8) can be found in the supplementary
402 information.

403

404 **4. Discussion**

405 Plaza et al. (1997) show, for the summer period in the study area, that the development of
406 strong thermal convective activity, and the influence of the mountain ranges produce
407 characteristic mesoscale re-circulations. On the other hand Crespí et al. (1995) report, also for
408 summer and the study area, the development of a very deep mixing layer. These authors
409 report that these re-circulations contribute markedly to the high O₃ episodes recorded in the
410 region. The arrangement of the Guadarrama range favours the early heating of its S slopes,
411 which causes a clockwise turning of wind direction, with a NE component during the night, E
412 and S during the early morning and midday, respectively, and SW during the late afternoon,
413 thus defining the north-western sector downwind of the city as the prone area for O₃
414 transport. Night-time downslope winds inside the basin induce the observed north-easterlies
415 at lower levels. Influenced by these contributions, the barrier effect of the Guadarrama range
416 against the N and NW (Atlantic) winds, as well as the repeated clockwise circulation described
417 above, cause the sloshing of the urban plume of Madrid across the basin. Regarding the
418 vertical scale, Plaza et al. (1997) also show that fumigation from high O₃-rich layers (injected by
419 upslope winds the previous day or days, or transported from other areas outside the MAB)
420 could also contribute to the enhancement of the surface O₃ concentrations across the basin.
421 This is attributed to the upward gradient in concentrations in the lower 1 km of the
422 atmosphere measured in the early morning and the subsequent mixing across the PBL at
423 midday. On the other hand, Gómez-Moreno et al. (2011) and Brines et al. (2015) report both
424 intensive summer and winter NPF episodes in the western border of Madrid City, often
425 simultaneously with the highest O₃ episodes.

426 Considering the free sounding- O₃ profiles in Figure 3, high O₃ concentrations (>70 ppb) can be
427 observed above the PBL, between 3000 and 5000 m a.s.l., which may be related to larger-scale
428 transport of pollutants, previously uplifted to the mid-troposphere or originated after a
429 stratospheric intrusion and a subsequent deep subsidence into the middle troposphere, as is
430 probably the case based on the ECMWF ERA-Interim reanalysis data. Transport of high O₃ air
431 masses in the middle troposphere, as for 13/07/2016 in Figure 3, was also documented by
432 Plaza et al. (1997) over this area in July 1994, during the final phase of a high O₃ period. More
433 recently, Kalabokas et al. (2013, 2015, 2017), Zanis et al. (2014), and Akritidis et al. (2016),
434 among others, have shown that similar transport processes of enriched O₃ layers at high
435 altitude can contribute to increased surface O₃ concentrations during the summer in the
436 Eastern Mediterranean. This transport has been associated with large-scale subsidence within
437 strong northerly winds in the Eastern Mediterranean (Etesian winds), and the affected layers
438 are dryer than average and show negative temperature anomalies. Figure S11 shows the
439 ECMWF ERA-Interim reanalysis together with the AEMET O₃ free soundings at Madrid airport
440 for 13/07/2016. The ridging at the lower troposphere over the Bay of Biscay at the rear of an
441 upper-level trough (left panels) is accompanied by intense NW winds blowing in the middle
442 and upper troposphere and NE winds at ground level and up to 2000 m (see the radiosonde
443 profile in the same figure). The O₃ intrusion is associated with the upper-level trough (Sections
444 A-A and B-B in the figure), and a large area of deep subsidence and extremely low relative
445 humidity observed within the NW flows over Madrid and to the north of the Iberian Peninsula
446 and the Bay of Biscay. High O₃ concentrations and low relative humidity of the ERA-Interim
447 profiles over the airport of Madrid (green and red dotted-lines in the panel “g” of Figure S11)
448 are in agreement with the radiosonde observations in the same panel.

449 The question now is how much of this O₃ could fumigate at ground level. According to the
450 radiosonde data, the mixing height top was about 2000 m a.s.l. at midday, but could increase
451 to about 3100 m a.s.l. after the projection of the surface temperature increase observed
452 during the afternoon at nearby stations. This height reaches the lower part of the O₃ enriched
453 layer originated in the tropopause folding. Thus, a certain impact seems likely. However, the
454 O₃ concentrations were relatively low at all surface stations during that day, as it corresponds
455 to a vented, low-O₃ period.

456 Thus, according to the O₃ soundings and radio-soundings analysed above, previous evidence
457 described by Plaza et al. (1997), and the surface air quality measurements presented here,
458 surface O₃ formation from precursor emissions within the MMA seems to develop in the core
459 of regional processes, modulated by large-scale meteorological conditions, distinguishing two
460 types of episodes:

- 461 • ACCUMULATION, occurring in stable, stagnant conditions and regional accumulation of
462 pollutants (in the sense of Millan et al., 1997, 2000; Gangoiti et al., 2001; Millán, 2014),
463 with high O₃ reserve strata accumulated during the previous day(s) in residual layer(s) and
464 associated with fumigation around midday of the following day. The O₃ concentrations are
465 high along the whole atmospheric column, but enriched in the lower section by additional
466 local formation of O₃ within the PBL and transport-recirculation of the urban plume of
467 Madrid around the area. This transport-recirculation is characterised by a net transport to
468 the NW-N during daytime, after vertical mixing, and to the S and SW during night-time,
469 inside the residual layer and decoupled from a more stable nocturnal surface layer.

470 Typically, pollutants accumulate during periods of 2-6 days, resulting in well-marked peak
471 and valley concentration periods that affect background, peri-urban, and in-city stations.
472 This is the case for the O₃-soundings of 29/06/2016 (not shown) and, particularly,
473 27/07/2016 (Figure 7) or the measurements with captive and free balloons by Plaza et al.
474 (1997) in 1993 and 1994, with very high concentrations of O₃ in the lower atmospheric
475 layers, usually forming a bump in the vertical profile of O₃ below a height of 2000 m a.s.l.,
476 easily reachable after daytime convection (Figure 7). As illustrated for 06/07/2017, OFP
477 (Table S1 and Figure S1) may be largely dominated by the carbonyls (mostly formaldehyde
478 and acetaldehyde), followed by aromatic compounds (benzene, toluene, and C₈,C₉, and
479 C₁₀ aromatics) when considering the VOC pool during the morning traffic peaks. The
480 influence of aromatic VOCs on OFP rapidly decreases, while the influence of biogenic VOCs
481 (mostly isoprene followed by monoterpenes as primary species, and methacrolein, methyl-
482 vinyl-ketone, isoprene-derived isomers of unsaturated hydroxy hydroperoxides (ISOPOOH)
483 and methylglyoxal, as the main secondary species) increases through the day, resulting in a
484 similar potential influence of biogenic and aromatic VOCs on O₃ formation during
485 accumulation periods, but with an OFP still dominated by carbonyls.

486 • VENTING, occurring in advective atmospheric conditions (in the sense of Millan et al., 1997,
487 2000; Gangoiti et al., 2001; Millán, 2014), with O₃-soundings characterized by (probably
488 external) contributions from high-altitude O₃ strata and their fumigation on the surface
489 (episodes 11-14/07/2016). There is no accumulation of pollutants above the stable
490 nocturnal boundary layer because more intense and steady winds swept out the local
491 production during the preceding day. OFP contributions of carbonyls (dominating OFP), and
492 aromatic and biogenic VOCs did not significantly vary for 13 and 14/07/2017 from what is
493 described above for 06/07/2017.

494 As detailed in Sections 3.1 and 3.2, with the weakening of general atmospheric circulation by
495 the end of the campaign period, O₃ and UFP smoothly and progressively accumulated in the
496 basin (Figure 5). An observed decrease of the PBL depth (up to ~1800 m at midday, according
497 to the AEMET radio-soundings during the campaign, see Figure S5) probably also contributed
498 to the progressive increase in pollutant concentrations through the campaign.

499 With respect to the vertical variability, the general pattern for UFP (N₃) clearly showed a rapid
500 and marked growth of the PBL in the first hours of daylight (Figure 8). In these early stages of
501 the day, O₃ profiles were characterized by a succession of strata of different concentrations,
502 but a clear increasing trend towards the higher levels (Figure 8). The discontinuity of the PBL
503 ceiling, reflected in the UFP, temperature, and humidity profiles, was not identified as such in
504 the O₃ profiles (Figures 5, 6, and S6 to S8). As the day progresses, the UFP and O₃
505 concentration profiles are homogenized and a progressive diurnal growth of O₃ concentrations
506 occurs until 16:00 or 17:00 UTC (Figure 8), most clearly observed at the surface. This vertical
507 variability points to different aspects, such as: (i) the relevance of fumigation from high
508 altitude O₃-rich strata; ii) surface titration by NO and deposition of O₃; (iii) surface
509 photochemical generation of O₃ from precursors (with higher concentrations close to the
510 surface); and (iv) horizontal O₃ and precursor surface transport from the urban plume of
511 Madrid towards MJDH-RC. The upper O₃-rich strata might have an external (to the Madrid
512 basin) origin or might have been injected regionally at high altitudes on the previous day(s) by
513 the complex re-circulations of air masses already reported by Millán et al. (1997, 2000, 2002),

514 EC (2002, 2004), Gangoiti et al. (2001), Mantilla et al. (1997), Castells et al. (2008a, 2008b), and
515 Millán (2014) for the WMB, by McKendry and Lundgren (2000) for other parts of the world,
516 and by Plaza et al. (1997), and Diéguez et al. (2007, 2014) for the Madrid area.

517 According to the last referenced authors, due to the orientation of the Sierra de Guadarrama
518 (Figure 1), the heating of its S slopes throughout the day forces the wind direction to veer,
519 describing an arc that sweeps the zones to the N of Madrid clockwise, from the W to the NE.
520 Dieguéz et al. (2014) show that the O₃ maxima are recorded at an intermediate point on this
521 route (El Pardo, Colmenar V., see location in Figures 9 and S12), which is determined by the
522 wind speed, initial composition of the urban plume, and results of photochemical processes on
523 its route from the metropolitan area to tens of kilometres away. In addition, our results and
524 those of Plaza et al. (1997) show that O₃ fumigation from high atmospheric layers decisively
525 contributes to the increases in the surface levels, since surface concentrations during our
526 measurements never exceeded those recorded at the highest altitude reached, and at midday
527 homogeneous O₃ levels are measured across the lower 1.2 km of the PBL.

528 During the whole month of July 2016, there was a clear veering of the urban plume from
529 Madrid, with night plume transport towards the SW (MJDH-San Martin de V., Figures 9 and
530 S12), and towards the NW, N-NE, and, in some cases, E-SE during the morning and midday,
531 followed by the decoupling and onset of the evening and nocturnal flow towards the SW. This
532 veering seems to be causally associated with the high O₃ levels recorded in the W to E areas
533 surrounding northern Madrid, since the peak concentrations recorded by the official air quality
534 network follow this spatial and temporal evolution (Figure S12) for the exceedances of the O₃
535 information threshold. These plume impacts occur in periods when the O₃ concentration is
536 already high because of accumulation from one day to the next in the (same) air mass, which is
537 not completely renewed due to general circulation conditions. The relevance of the latter has
538 been recently demonstrated by Otero et al. (2016), who report the maximum temperature as
539 the parameter more directly related with high O₃ concentrations in Central Europe, whereas,
540 in the WMB region, the O₃ concentrations were more related to the concentrations recorded
541 the day before.

542 On the other hand, the differential afternoon-evening decrease of O₃ surface concentrations,
543 compared with those found at the top of the soundings again demonstrates the relevance of
544 high-altitude layers and their fumigation to the surface in the hours of maximum convection.

545 Regarding the concentrations of UFP, they were very homogeneous throughout the PBL during
546 the vertical profiles, especially in the hours of maximum convection, showing a marked
547 increase from 11 to 14/07/2016 for the whole depth for all profiles (Figure 8). Thus, on the
548 12/07/2016, the upper limit of the PBL (marked by a sharp reduction in UFP levels) reached
549 900 and 1200 m a.g.l., respectively, in the soundings conducted at 08:05 and 10:12 UTC (Figure
550 8). In turn, on 14/07/2016, the top of the PBL exceeded 1200 m a.g.l. only in the afternoon,
551 being constrained to 300 to 700 m a.g.l. from 08:05 and 10:45 h UTC (also shown in the
552 progressive loss of -1800 m in the midday PBL height from 11 to 14/07/2016, revealed by
553 AEMET radio-soundings).

554 The enhanced convection on 12/07/2016 probably favoured the dilution of UFP concentrations
555 and reinforced the fumigation of O₃ from the upper levels. Conversely, the lower development
556 of the PBL on 14/07/2016, causing less surface UFP dilution and lower top-down contributions

557 to O₃ surface concentrations, accounted for the opposite O₃ and UFP profiles. Thus, a weaker
558 development of the PBL might result in the increase of UFP concentrations, even if UFP
559 emission/formation rates did not vary significantly. However, we cannot discard the possibility
560 that this UFP increase on the last day was the result of a higher intensity and duration of the
561 nucleation episodes.

562 Consideration of the evolution of surface O₃ concentrations on 11 and 12/07/2016 (as shown
563 in Figure 9), depicts a double wave: the first peak around midday (11:00-14:00 UTC on the first
564 day, and 12:00-13:00 on the second), and the second peak in the afternoon-evening (19-22:00
565 and 16:00-20:00 UTC, respectively), showing relative peaks (sometimes just a plateau). We
566 interpret that the morning increase of O₃ concentrations is dominated by both local
567 production and anthropogenic VOCs (Figure S1), and fumigation of upper levels, with an early
568 maximum when layers above are rich in O₃, which progressively decreases with dilution with
569 surface concentrations. The secondary evening concentration peak corresponds to the
570 advection of a locally enriched O₃ air mass (titration always causes O₃ depletion towards
571 nocturnal values). When both processes (morning fumigation and evening advection) are not
572 so strong, O₃ local production results in a more “typical” diurnal time evolution, with a single
573 maximum at 15:00-16:00 UTC, as seen on 13-14/07/2016 (Figure 9).

574 The relative importance of the local contribution of the MMA to the O_x concentrations
575 registered in the monitoring stations has also been evaluated by comparing the observations
576 at upwind and downwind locations relative to the city. In this respect, Atazar and Alcobendas
577 (Figure 9) are located downwind for 11 and 12/07/2016, and MJDH and Fuenlabrada are
578 upwind, while the opposite occurs for 13 and 14/07/2016. As the urban air mass is transported
579 towards the E and NE during the first two days, a local O_x contribution is superimposed on the
580 background at Atazar and Alcobendas, where recorded O_x was the highest in the basin (Figure
581 9). The contrary holds during the next two days, when these sites show lower concentrations
582 than the rest. MJDH and Fuenlabrada show a reversed behaviour, with lower concentrations
583 during the first two days and higher for the last days.

584 In addition of the local O₃, the background contribution can also be very relevant. At high
585 elevation, changes in the background tropospheric O₃ can be attributed to: (i) hemispheric
586 background concentrations, (ii) exchange between the free troposphere and boundary layer,
587 and iii) stratospheric inputs (Chevalier et al., 2007; Kulkarni et al., 2011; Parrish et al., 2012;
588 Lefohn et al., 2012; Kalabokas et al., 2013, 2015, 2017; Zanis et al., 2014; Akritidis et al., 2016;
589 Sicard et al., 2017).

590

591

592

593 **5. Conclusions**

594 The phenomenology of O₃ episodes in the Madrid Metropolitan Area (MMA, Central Iberia)
595 has been characterised. We found that O₃ episodes linked with precursors emitted in the
596 Madrid conurbation are modulated by the complex regional atmospheric dynamics.

597 Vertical profiles (up to 1200 m a.g.l.), obtained using tethered balloons and miniaturised
598 instrumentation at Majadahonda (MJDH), a sub-urban site located on the southwestern flank
599 of the Madrid Metropolitan Area (MMA) during 11-14/07/2016, showed how critical evolve
600 with altitude. Simultaneously, measurements of air quality and meteorological parameters
601 were carried out at 3 supersites within the MMA, where spatial differences highlight the
602 influence of atmospheric dynamics on different scales.

603 The results presented here confirm prior findings regarding the concatenation of relatively low
604 (venting) and high (accumulation) O₃ episodes in summer. In the Madrid Air Basin (MAB),
605 during both types of episodes, fumigation of high altitude O₃-rich layers (from a remote or
606 regional origin) contributes a relevant fraction to surface O₃ concentrations. Moreover, we
607 propose here a conceptual model (shown in Figure 10). To be specific:

608 • Accumulation episodes are activated by a relatively thinner PBL (< 1500 m a.g.l. at
609 midday), light synoptic winds, and the development of anabatic winds along the slope of
610 the Sierra de Guadarrama (W and NW of MAB, with >2400 m a.g.l. peaks). This PBL height,
611 lower than the mountain range, and the development of the mountain breezes cause the
612 vertical recirculation of air masses, enrichment of O₃ in the lower troposphere, as well as
613 the formation of reservoir layers that fumigate to the surface as the diurnal convective
614 circulation develops. This dynamics accounts for the occurrence of the high O_x (O₃+NO₂)
615 surface concentrations.

616 • During venting episodes, with more intense synoptic winds, and the top of the PBL usually
617 reaching >2000 m a.g.l., vertical O₃ profiles were characterised by an upward increase in
618 concentrations (whereas lower-altitude O₃ maxima were observed in the accumulation
619 periods). Interestingly, vertical profiles demonstrated that, during the study period, O₃
620 fumigation (top-down) from upper layers prevailed as a contribution to surface O₃
621 concentrations, whereas the increase of UFP takes place bottom-up, progressing with the
622 development of the PBL and the occurrence of nucleation and growth episodes occurring
623 within the PBL. Thus, crossing the boundary of the PBL from the free troposphere
624 increases of UFP concentrations by an order of magnitude, and slight decreases in O₃
625 levels were registered. This O₃ and UFP vertical distribution through the day is consistent
626 with the existence of an efficient venting mechanism which is able to sweep out the local
627 production of the day. Thus, there is no accumulation of pollutants above the observed
628 stable nocturnal boundary layer from one day to the next, and new UFP production is
629 added from below the following day. The presence of O₃-enriched layers well above the
630 stable nocturnal boundary layer, transported by sustained intense westerly winds,
631 suggests a remote origin of this pollutant, after photochemical reactions and uplift
632 processes developed at least the day before away from the MAB, or stratospheric
633 intrusions, such as the one documented on 13/07/2016, during the field campaign.
634 However, surface O₃ concentrations at all stations of the MAB were low during this day;
635 consequently, even when fumigation from this intrusion was very likely, its air quality
636 affection was irrelevant for the same days, but the effect in the forthcoming days of
637 subsided O₃ cannot be evaluated with our tools. The high-O₃ period in the area initiated
638 the day after, 14/07/2016, and attained its highest concentration on 16/07/2016.

639 The results obtained in this intensive field campaign can be summarized in the following
640 conclusions and recommendations concerning O₃ abatement policies:

641 • The O₃ source apportionment is very complex, with contributions from local/regional and
642 remote sources, including the stratosphere. The relative contributions of these might vary
643 in time and space (e.g. Lefohn et al., 2014).

644 • Climate change might reduce the benefits of the O₃ abatement policies (since heat waves
645 increase O₃ episodes). This, as well as the measures and policies in Northern America and
646 Asia, will need to be considered in future Europe policies for O₃ mitigation (Lefohn and
647 Cooper, 2015; Sicard et al., 2017).

648 • The phenomenology of O₃ episodes in the WMB is extremely complex, mainly due to the
649 close coupling between photochemistry processes and mesoscale atmospheric dynamics.
650 This requires, consequently, abatement policies very different from the ones useful for
651 Central and Northern Europe, as intensive research has demonstrated in the last decades.

652 • In the MAB, during the highest O₃ (accumulation) episodes, in addition to the contribution
653 (to surface concentrations) by fumigation of upper O₃ (from regional transport,
654 hemispheric free troposphere O₃, and intruded stratospheric O₃, X in Figure 10), there is
655 an added fraction produced locally and transported-recirculated within the MAB, which
656 accumulates from one day to the next (Y in Figure 10). If sensitivity analyses demonstrate
657 that abatement of specific precursors would have an effect on reducing O₃ peaks, then
658 the reduction strategies (geographic extension, timing, and so on) for decreasing the X
659 and Y components are very different, and, in most cases, the X component will dominate
660 the relative contributions. Thus, probably, structural measures over wider regions would
661 be more effective than local episodic measures (which might have a larger effect on the Y
662 component). In terms of precursors, the OFP analysis carried out at the ISCIII site shows
663 that, even if anthropogenic emissions may dominate the O₃ formation through the
664 potential impact of alkenes and alkanes (not measured) and the high contribution of
665 carbonyls (formaldehyde and acetaldehyde), biogenic emissions must be considered.
666 Biogenic VOC (primary and secondary) and aromatic compounds (C6 to C10) contribute to
667 the same extent to the OFP, according our calculations (Table S1 and Figure S1).

668 • The meteorological scenarios causing the summer accumulation episodes in the MAB
669 (high temperatures, low synoptic winds, and relatively thinner PBL) should be forecast in
670 order to drive an effective alert system.

671 • A more detailed characterisation of O₃ precursors (VOC and BVOCs) in the MAB is
672 necessary, especially in the source areas, to effectively predict the photochemical
673 evolution of the plumes, the main impact areas where O₃ from high-altitude reservoir
674 layers formed the previous day(s) fumigates to the surface levels enriched in O₃ and other
675 precursors.

676 • Modelling techniques and sensitivity analyses will allow the simulation of real conditions
677 concerning O₃ abatement potential only if the following is achieved in advance: i) the
678 recirculation cells and other local/regional meteorological processes, such as the
679 fumigation timing and regional plume transport, are reproduced; ii) a geographically
680 resolved and accurate emission inventory of O₃ precursors in the source areas and their

681 temporal modulation is included; and iii) the origin of the high- altitude O₃ strata from
682 external origins is reproduced.

683 • A good combination of regional/local scale modelling, able to reproduce
684 horizontal/vertical re-circulations of air masses and the behaviour of urban/industrial
685 plumes in complex topography/meteorology, with modelling able to calculate
686 contributions from long-range transport, free troposphere, and stratospheric O₃ will be
687 needed to efficiently support policy (see, for example, the ACP special issue on the
688 Atmospheric Chemistry and Climate Model Inter-comparison Project, ACCMIP
689 https://www.atmos-chem-phys.net/special_issue296.html; the FAIRMODE initiative,
690 Thunis et al., 2015; or the Monitoring Atmospheric Composition & Climate (MACC)).

691 The conceptual model described in this study for O₃ episodes in the MMA confirms the
692 relevance of the vertical re-circulations (on top of the high atmospheric multi-source O₃
693 background) that Millan et al. (1997, 2000), Gangoiti et al. (2001), and Millán (2014)
694 highlighted, controlled in this case by specific synoptic conditions and the PBL depth, may also
695 be applicable to most of the Western Mediterranean Basin (WMB). Thus, Otero et al. (2016)
696 demonstrate that, in Central Europe, the highest temperature is the most statistically related
697 parameter for O₃ episodes, whereas in the WMB it is the O₃ level recorded the day before
698 (reflecting re-circulation).

699

700 **Acknowledgements**

701 The present work was supported by the Spanish Ministry of Agriculture, Fishing, Food and
702 Environment, Madrid City Council and Madrid Regional Government, and by the Ministry of
703 Economy, Industry and Competitiveness and FEDER funds under the project HOUSE (CGL2016-
704 78594-R), and by the Generalitat de Catalunya (AGAUR 2017 SGR41). Part of this research was
705 supported by the Korea Ministry of Environment through "The Eco-Innovation project". The
706 support of the CUD of Zaragoza (project CUD 2016-05), UPV/EHU (UFI 11/47, GIU 16/03), the
707 project PROACLIM CGL2014-52877-R, the City Council of Majadahonda for logistic support and
708 AEMET for providing surface meteorological data, and data from radiosoundings and ozone
709 free-soundings is also acknowledged. We thank Alava Ingenieros, TSI, Solma Environmental
710 Solutions, and Airmodus for their support, and María Díez for her computer support in the
711 treatment of radiosonde data.

712

713 **6. References**

714 Akritidis D., Pozzer A., Zanis P., Tyrllis E., Škerlak B., Sprenger M., Lelieveld J., 2016. On the role
715 of tropopause folds in summertime tropospheric ozone over the eastern Mediterranean and
716 the Middle East. *Atmos. Chem. Phys.* 16, 14025–14039.

717 Brines M., Dall'Osto M., Beddows D.C.S., Harrison R.M., Gómez-Moreno F., Núñez L., Artíñano
718 B., Costabile F., Gobbi G.P., Salimi F., Morawska L., Sioutas C., Querol X., 2015. Traffic and
719 nucleation events as main sources of ultrafine particles in high-insolation developed world
720 cities. *Atmos. Chem. Phys.* 15, 5929-5945.

721 Carslaw, D. C., Ropkins K., 2012. Openair --- an R package for air quality data analysis. Environ.
722 Modelling & Software 27-28, 52-61.

723 Carslaw D.C., Murrells T.P., Andersson J., Keenan M., 2016. Have vehicle emissions of primary
724 NO₂ peaked? Faraday Discuss. 189, 439-454.

725 Castell N., Mantilla E., Millán M.M., 2008a. Analysis of tropospheric ozone concentration on a
726 Western Mediterranean site: Castellon (Spain). Environ. Monit. Assess. 136, 3-11.

727 Castell N., Stein A.F., Salvador R., Mantilla E., Millán M.M., 2008b. The impact of biogenic VOC
728 emissions on photochemical ozone formation during a high ozone pollution episode in the
729 Iberian Peninsula in the 2003 summer season. Advances in Sci. Res. 2, 9-15.

730 Castell N., Tellez L., and Mantilla E., 2012. Daily, seasonal and monthly variations in ozone
731 levels recorded at the Turia river basin in Valencia (Eastern Spain). Environmental Science and
732 Poll. Res. 19, 3461-3480.

733 Chevalier A., Gheusi F., Delmas R., Ordóñez C., Sarrat C., et al., 2007. Influence of altitude on
734 ozone levels and variability in the lower troposphere: a ground-based study for Western
735 Europe over the period 2001-2004. Atmos. Chem. Phys. 7, 4311-4326.

736 Crespi S.N., Artíñano B., Cabal H., 1995. Synoptic classification of the mixed-layer height
737 evolution. J. App. Meteorol. 34, 1668-1677.

738 Dieguez J.J., Calatayud V., Mantilla E., 2014. CEAM Report for the Ministry of Agriculture, Food
739 and Environment, Fundación Biodiversidad. Informe Final. Memoria Técnica Proyecto CONOZE.
740 CONtaminación por OZono en España. 137 pp [http://www.magrama.gob.es/es/calidad-y-](http://www.magrama.gob.es/es/calidad-y-evaluacion-ambiental/temas/atmosfera-y-calidad-del-aire/Informe_t%C3%A9cnico_CONOZE%5B1%5D_tcm7-330956.pdf)
741 [evaluacion-ambiental/temas/atmosfera-y-calidad-del-](http://www.magrama.gob.es/es/calidad-y-evaluacion-ambiental/temas/atmosfera-y-calidad-del-aire/Informe_t%C3%A9cnico_CONOZE%5B1%5D_tcm7-330956.pdf)
742 [aire/Informe_t%C3%A9cnico_CONOZE%5B1%5D_tcm7-330956.pdf](http://www.magrama.gob.es/es/calidad-y-evaluacion-ambiental/temas/atmosfera-y-calidad-del-aire/Informe_t%C3%A9cnico_CONOZE%5B1%5D_tcm7-330956.pdf)

743 Dieguez J.J., Millán M., Padilla L., Palau J.L., 2009. Estudio y evaluación de la contaminación
744 atmosférica por ozono troposférico en España. CEAM Report for the Ministry of Agriculture,
745 Food and Environment, INF FIN/O3/2009. 372 pp. [http://www.magrama.gob.es/es/calidad-y-](http://www.magrama.gob.es/es/calidad-y-evaluacion-ambiental/temas/atmosfera-y-calidad-del-aire/8_A_Informe_final_ozono-ceam_Julio_2009_tcm7-152609.pdf)
746 [evaluacion-ambiental/temas/atmosfera-y-calidad-del-aire/8_A_Informe_final_ozono-](http://www.magrama.gob.es/es/calidad-y-evaluacion-ambiental/temas/atmosfera-y-calidad-del-aire/8_A_Informe_final_ozono-ceam_Julio_2009_tcm7-152609.pdf)
747 [ceam_Julio_2009_tcm7-152609.pdf](http://www.magrama.gob.es/es/calidad-y-evaluacion-ambiental/temas/atmosfera-y-calidad-del-aire/8_A_Informe_final_ozono-ceam_Julio_2009_tcm7-152609.pdf)

748 Directive 2008/50/EC of the European Parliament and of the council of 21 May 2008 on
749 ambient air quality and cleaner air for Europe.

750 Directive 2015/1480 of 28 August 2015 amending several annexes to Directives 2004/107/EC
751 and 2008 /50/EC of the European Parliament and of the Council laying down the rules
752 concerning reference methods, data validation and location of sampling points for the
753 assessment of ambient air quality.

754 Doval M., Castell N., Téllez L., and Mantilla E., 2012. The use of experimental data and their
755 uncertainty for assessing ozone photochemistry in the Eastern Iberian Peninsula.
756 Chemosphere 89, 796-804.

757 EC, 2002. Ozone dynamics in the Mediterranean Basin: A collection of scientific papers
758 resulting from the MECAPIP, RECAPMA and SECAP Projects. Air Pollution Report 78. DG RTD
759 I.2, LX 46 2/82, B-1049 Brussels.

760 EC, 2004. European Commission Decision of 19 March 2004 "Concerning guidance for
761 implementation of Directive 2002/3/EC of the European Parliament and the Council relating to
762 ozone in ambient air (2004/279/EC). Official Journal of the European Union L87/50 of
763 25.3.2004.

- 764 EEA, 2017. Air quality in Europe-2017 report. EEA Report, No 13/2017. ISBN 978-92-9213-920-
765 9, Luxembourg: Publications Office of the European Union, 74 pp.
766 <https://www.eea.europa.eu/publications/air-quality-in-europe-2017>
- 767 EMEP, 2016. Air pollution trends in the EMEP region between 1990 and 2012. EMEP/CCC-
768 Report 1/2016, ISBN : 978-82-425-2834-6, 107 pp.
- 769 Escudero M., Lozano A., Hierro J., del Valle J., Mantilla E., 2014. Urban influence on increasing
770 ozone concentrations in a characteristic Mediterranean agglomeration. *Atmos. Environ.* 99,
771 322–332.
- 772 Gangoiti G., Millán M.M., Salvador R., and Mantilla E., 2001. Long-range transport and re-
773 circulation of pollutants in the western Mediterranean during the project Regional Cycles of Air
774 Pollution in the West-Central Mediterranean Area. *Atmos. Environ.* 35, 6267-6276.
- 775 Garcia Dos Santos S., Benarroch Benarroch R., Fernández Patier R., Sintes Puertas M.A.,
776 Cantón Gálvez J.M., Alonso Herreros J. y Guevara Hernández S. 2014. Atmospheric Pollution in
777 North Africa. Facts and lessons in the Spanish City of Ceuta. 9TH International Conference on
778 Air Quality Science and Application. Garmish (Germany) March 24 – 28.
- 779 Gerasopoulos E., Kouvarakis G., Vrekoussis M., Kanakidou M., Mihalopoulos N., 2005. Ozone
780 variability in the marine boundary layer of the Eastern Mediterranean based on 7-year
781 observations. *J. Geophys. Res.*, 110, D15309, doi:10.1029/2005JD005991.
- 782 Giannakopoulos C., Le Sager P., Bindi M., Moriondo M., Kostopoulou E., Goodess, C.M., 2009.
783 Climatic changes and associated impacts in the Mediterranean resulting from a 2 oC global
784 warming. *Global and Planetary Change* 68, 209-224.
- 785 Gómez-Moreno F.J., Pujadas M., Plaza J., Rodríguez-Maroto J.J., Martínez-Lozano P., Artíñano
786 B., 2011. Influence of seasonal factors on the atmospheric particle number concentration and
787 size distribution in Madrid, *Atmos. Environ.* 45, 3199-3180.
- 788 Kalabokas P.D., Viras, L.G., Bartzis, J.G., Repapis, C.C., 2000. Mediterranean rural ozone
789 characteristics around the urban area of Athens. *Atmos. Environ.* 34, 5199–5208.
- 790 Kalabokas P.D., Repapis C.C., 2004. A climatological study of rural surface ozone in central
791 Greece. *Atmos. Chem. Phys.*, 4, 1139–1147.
- 792 Kalabokas P.D., Mihalopoulos N., Ellul R., Kleanthous S., Repapis C.C., 2008. An investigation of
793 the meteorological and photochemical factors influencing the background rural and marine
794 surface ozone levels in the Central and Eastern. Mediterranean. *Atmos. Environ.* 42, 7894-
795 7906.
- 796 Kalabokas, P.D., Cammas, J.P., Thouret, V., Volz-Thomas, A., Boulanger, D., Repapis, C.C., 2013.
797 Examination of the atmospheric conditions associated with high and low summer ozone levels
798 in the lower troposphere over the eastern Mediterranean. *Atmos. Chem. Phys.* 13, 10339–
799 10352.
- 800 Kalabokas, P.D., Thouret, V., Cammas, J.P., Volz-Thomas, A., Boulanger, D., and Repapis, C.C.,
801 2015. The geographical distribution of meteorological parameters associated with high and
802 low summer ozone levels in the lower troposphere and the boundary layer over the Eastern
803 Mediterranean (Cairo case). *Tellus B*, 67, 27853.
- 804 Kalabokas P.D., Hjorth J., Foret G., Dufour G., Eremenko M., Siour G., Cuesta J., Beekmann M.,
805 2017. An investigation on the origin of regional springtime ozone episodes in the western
806 Mediterranean. *Atmos. Chem. Phys.* 17, 3905–3928.
- 807 Kourtidis K., Zerefos C., Rapsomanikis S., Simeonov V., Balis D., Perros P. E., Thomson A. M.,
808 Witte J., Calpini B., Sharobiem W. M., Papayianis A., Mihalopoulos N., Drakou R., 2002.

809 Regional levels of ozone in the troposphere over eastern Mediterranean. *J. Geophys. Res.*,
810 107, 8140, doi:10.1029/2000JD000140.

811 Kouvarakis G., Vrekoussis M., Mihalopoulos N., Kourtidis K., Rappenglueck B., Gerasopoulos E.,
812 Zerefos C., 2002. Spatial and temporal variability of tropospheric ozone in the boundary layer
813 above the Aegean Sea (eastern Mediterranean). *J. Geophys. Res.*, 107, 8137,
814 doi:10.1029/2000JD000081.

815 Kulkarni P.S., Bortoli D., Salgado R., Anton M., Costa M.J., et al., 2011. Tropospheric ozone
816 variability over the Iberian Peninsula. *Atmos. Environ.* 45, 174-182.

817 Kulmala M., Pirjola L., Mäkelä J.M., 2000. Stable Sulphate Clusters as a Source of New
818 Atmospheric Particles. *Nature* 404, 66-69.

819 Kulmala M., Vehkamehk H., Pet P.T., Dal Maso M., Lauri A., Kerminen V.-M., Birmili W.,
820 McMurry P., 2004. Formation and growth rates of ultrafine atmospheric particles: a review of
821 observations. *J. Aerosol Sci.* 35, 143-176.

822 Kulmala M., Kerminen V.M, 2008. On the formation and growth of atmospheric nanoparticles,
823 *Atmos. Res.* 90, 132-150.

824 Lee, H.-K., Hwang, I.-K., Ahn, K.-H., 2014. Development and Evaluation of Hy-CPC. *Particle and*
825 *Aerosol Research* 10, 93-97.

826 Lefohn A.S., Wernli H., Shadwick D., Oltmans S.J., Shapiro M., 2012. Quantifying the frequency
827 of stratospheric-tropospheric transport affecting enhanced surface ozone concentrations at
828 high- and low-elevation monitoring sites in the United States. *Atmos. Environ.* 62, 646-656.

829 Lefohn A. S., Emery C., Shadwick D., Wernli H., Jung J., Oltmans S. J., 2014. Estimates of
830 background surface ozone concentrations in the United States based on model-derived source
831 apportionment. *Atmos. Environ.* 84, 275–288.

832 Lefohn A.S., Cooper O.R, 2015. Introduction to the Special Issue on Observations and Source
833 Attribution of Ozone in Rural Regions of the Western United States. *Atmos. Environ.* 109, 279-
834 281.

835 Lelieveld J., Berresheim H., Borrmann S., Crutzen P.J., Dentener F.J., Fischer H., Feichter J., et
836 al., 2002. Global air pollution crossroads over the Mediterranean. *Science* 298, 794-799. MACC
837 (2018). Monitoring Atmospheric Composition & Climate. [http://www.gmes-](http://www.gmes-atmosphere.eu/services/raq/raq_nrt/)
838 [atmosphere.eu/services/raq/raq_nrt/](http://www.gmes-atmosphere.eu/services/raq/raq_nrt/)

839 Mantilla E., Millán M.M., Sanz M.J., Salvador R., and Carratalá A., 1997. Influence of
840 mesometeorological processes on the evolution of ozone levels registered in the Valencian
841 Community. In: I Technical workshop on ozone pollution in southern Europe. Valencia.

842 McKendry I.G., Lundgren J., 2000. Tropospheric layering of ozone in regions of urbanized
843 complex and/or coastal terrain: a review. *Progress in Physical Geography* 24, 3.

844 Millán M.M., Artiñano B., Alonso L., Navazo M., Castro M., 1991. The effect of meso-scale
845 flows on regional and long-range atmospheric transport in the Western Mediterranean area.
846 *Atmos. Environ.* 25A, 5/6, 949-963.

847 Millán M.M., Salvador R., Mantilla E., Artiñano B., 1996a. Meteorology and photochemical air
848 pollution in southern Europe: experimental results from EC research projects. *Atmos. Environ.*
849 30, 1909-1924.

850 Millán M.M., Mantilla E., Salvador R., Kallos G., 1996b. Regional and long-range transport
851 scenarios for photo-oxidants on the Mediterranean basin in summer. Ninth joint conference
852 on applications of air pollution meteorology. 438-441. Am. Meteorol Soc., Boston.

- 853 Millán M.M., Salvador R., Mantilla E., 1996c. Mesoscale processes and photo-oxidants cycles
854 on the Spanish Mediterranean coast. Ninth joint conference on applications of air pollution
855 meteorology.434-437. Am. Meteorol. Soc., Boston.
- 856 Millán M.M., Salvador R., Mantilla E., and Kallos G., 1997. Photooxidant dynamics in the
857 Mediterranean basin in summer: Results from European research projects. J. Geophys. Res.
858 102, 8811-8823.
- 859 Millán M.M. , Sanz M. J., 1999. Ozone in Mountainous regions and in Southern Europe. In: Ad
860 hoc Working group on Ozone Directive and Reduction Strategy Development, (eds.). Ozone
861 Position Paper 145-150. European Commission, Brussels.
- 862 Millán M.M., Mantilla E., Salvador R., Carratalá A., Sanz M.J., Alonso L., Gangoiti G., Navazo M.,
863 2000. Ozone Cycles in the Western Mediterranean Basin: Interpretation of Monitoring Data in
864 Complex Coastal Terrain. J. App. Meteorol. 39, 487-508.
- 865 Millán M.M., Sanz M.J., Salvador R., Mantilla E., 2002. Atmospheric dynamics and ozone cycles
866 related to nitrogen deposition in the western Mediterranean. Environ. Poll. 118, 167-186.
- 867 Millán M.M., 2002. Ozone dynamics in the Mediterranean basin. A collection of scientific
868 papers resulting from the MECAPIP, RECAPMA and SECAP Projects. Air Pollution Research
869 Report 78.Fundación Centro de Estudios Ambientales del Mediterráneo - CEAM. Valencia,
870 España. 287 pp.
- 871 Millán M.M. 2014. Extreme hydrometeorological events and climate change predictions in
872 Europe. J. Hydrol. 518B, 206-224.
- 873 Minguillón M.C., Brines M., Pérez N., Reche C., Pandolfi M., Fonseca A.S., Amato F., Alastuey
874 A., Lyasota A., Codina B., Lee H.-K., Eun H.-R., Ahn K.-H., Querol X., 2015. New particle
875 formation at ground level and in the vertical column over the Barcelona area. Atmos. Res. 164–
876 165, 118–130.
- 877 Monks P.S., Archibald A.T., Colette A., Cooper O., Coyle M., Derwent R., Fowler D., Granier C.,
878 Law K.S., Mills G.E., Stevenson D.S., Tarasova O., Thouret V., von Schneidemesser E.,
879 Sommariva R., Wild O., Williams M.L., 2015. Tropospheric ozone and its precursors from the
880 urban to the global scale from air quality to short-lived climate forcer. Atmos. Chem. Phys., 15,
881 8889-8973.
- 882 Ochoa-Hueso R., Munzi S., Alonso R., Arróniz-Crespo M., Avila A., Bermejo V., Bobbink R.,
883 Branquinho C., Concostrina-Zubiri L., Cruz C., Cruz de Carvalho R., De Marco A., et al., 2017.
884 Ecological impacts of atmospheric pollution and interactions with climate change in terrestrial
885 ecosystems of the Mediterranean Basin: Current research and future directions. Environ. Poll.,
886 227, 194-206.
- 887 Otero N., Sillmann J., Schnell J.L., Rust H., Butler T., 2016. Synoptic and meteorological drivers
888 of extreme ozone concentrations over Europe. Environ. Res. Lett. 11, 024005.
- 889 Pandolfi M., Tobías A., Alastuey A., Sunyer J., Schwartz J., Lorente J., Pey J., Querol X., 2014.
890 Effect of atmospheric mixing layer depth variations on urban air quality and daily mortality
891 during Saharan dust outbreaks. Sci. Total Environ. 494-495, 283-289.
- 892 Paoletti E., De Marco A., Beddows D.C.S., Harrison R.M., Manning W.J., 2014. Ozone levels in
893 European and USA cities are increasing more than at rural sites, while peak values are
894 decreasing. Environ. Poll. 192, 295-299.
- 895 Parrish D.D., Law K.S., Staehelin J., Derwent R., Cooper O.R., et al., 2012. Long-term changes in
896 lower tropospheric baseline ozone concentrations at northern mid-latitudes. Atmosph. Chem.
897 Phys. 12, 11485-11504.

- 898 Plaza J., Pujadas M., Artíñano B., 1997. Formation and Transport of the Madrid Ozone Plume. J.
899 Air & Waste Management Association 47, 766-774.
- 900 Querol X., Alastuey A., Pandolfi M., Reche C., Pérez N., Minguillón M.C., Moreno T., Viana M.,
901 Escudero M., Orío A., Pallarés M. and Reina F., 2014, '2001–2012 trends on air quality in Spain',
902 Science Total Environment 490, 957–969.
- 903 Querol X., Alastuey A., Orío A., Pallares M., Reina F., Dieguez JJ., Mantilla E., Escudero M.,
904 Alonso L., Gangoiti G., Millán M., 2016. On the origin of the highest ozone episodes in Spain. .
905 Sci. Total Environ. 572, 379-389.
- 906 Querol X., Gangoiti G., Mantilla E., Alastuey A., Minguillón M. C., Amato F., Reche C., Viana M.,
907 Moreno T., Karanasiou A., Rivas I., Pérez N., Ripoll A., Brines M., Ealo M., Pandolfi M., Lee H.-K.,
908 Eun H.-R., Park Y.-H., Escudero M., Beddows D., Harrison R.M., Bertrand A., Marchand N.,
909 Lyasota A., Codina B., Olid M., Udina M., Jiménez-Esteve B., Soler M.R., Alonso L., Millán M.,
910 Ahn, K.-H., 2017. Phenomenology of high-ozone episodes in NE Spain. Atmos. Chem. Phys. 17,
911 2817-2838
- 912 Reche C., Moreno T., Amato F., Pandolfi M., Pérez J., de la Paz D., Díaz E., Gómez-Moreno F.J.,
913 Pujadas M., Artíñano B., Reina F., Orío A., Pallarés M., Escudero M., Tapia O., Crespo E.,
914 Vargas R., Alastuey A., Querol X., 2018. On the complexity of Spatial and time dependence of
915 high ozone events in central Spain. Atmos. Environ., submitted.
- 916 Saha, S.; S. Moorthi, X. Wu, J. Wang, S. Nadiga, P. Tripp, D. Behringer, Y. T. Hou, H. Y. Chuang,
917 M. Iredell, M. Ek, J. Meng, R. Yang, M. Peña Mendez, , H. van den Dool, Q. Zhang, W. Wang, M.
918 Chen, and E. Becker, 2014. The NCEP Climate Forecast System Version 2. Journal of Climate,
919 27, 2185–2208.
- 920 Saiz-Lopez, A., Borge, R., Notario, A., Adame, J.A., De la Paz, D., Querol, X., Artíñano, B.,
921 Gomez-Moreno, F.J., Cuevas, C.A., 2017. Unexpected increase in the oxidation capacity of the
922 urban atmosphere of Madrid, Spain, Sci. Rep, 7, 45956, doi:10.1038/srep45956.
- 923 Salma I, Németh Z, Kerminen V-M, Aalto P, Nieminen T, Weidinger T, Molnár Á, Imre K,
924 Kulmala M., 2016. Regional effect on urban atmospheric nucleation, Atmos. Chem. Phys. 16,
925 8715-8728.
- 926 Salvador R., Millán M.M., Mantilla E., Baldasano J.M., 1997. Mesoscale modelling of
927 atmospheric processes over the western Mediterranean area during summer. International
928 Journal of Environ. Poll. 8, 513-528.
- 929 Salvador R., Millán M.M., Calbo J., 1999. Horizontal Grid Size Selection and its influence on
930 Mesoscale Model Simulations. J. App. Meteorol. 38, 1311-1329.
- 931 Salvador P., Artíñano B., Viana M., Alastuey A., Querol X., 2015. Multicriteria approach to
932 interpret the variability of the levels of particulate matter and gaseous pollutants in the
933 Madrid metropolitan area, during the 1999-2012 period. Atmos. Environ. 109, 205-216.
- 934 Sicard P., De Marco A., Troussier F., Renou C., Vas N., Paoletti E., 2013. Decrease in surface
935 ozone concentrations at Mediterranean remote sites and increase in the cities. Atmos.
936 Environ. 79, 705-715. Sicard P., Anav A., De Marco A., Paoletti E., 2017. Projected global
937 tropospheric ozone impacts on vegetation under different emission and climate scenarios.
938 Atmos. Chem. Phys. 17, 12177–12196.
- 939 Sipilä M., Berndt T., Petäjä T., Brus D., Vanhanen J., Stratmann F., et al. 2010. The role of
940 sulfuric acid in atmospheric nucleation. Science 327, 5970, 1243-1246.
- 941 Stein A.F., Mantilla E., Millán M.M., 2004. Ozone formation downwind an industrial complex in
942 the western Mediterranean. In: 13th World Clean Air and Environmental Protection, August
943 22-27. London, U.K.

- 944 Stein A.F., Mantilla E., and Millán M.M., 2005. Using measured and modelled indicators to
945 assess ozone-NO_x-VOC sensitivity in a western Mediterranean coastal environment. *Atmos.*
946 *Environ.* 39, 7167-7180.
- 947 Thunis P., Pisonia E., Degraeuwe B., Kranenburg R., Schaap M., Clappier S., 2015. Dynamic
948 evaluation of air quality models over European regions. *Atmos. Environ.* 111, 185-194.
- 949 Velchev K., Cavalli F., Hjorth J., Marmer E., Vignati E., Dentener F., Raes F., 2011. Ozone over
950 the Western Mediterranean Sea e results from two years of shipborne measurements. *Atmos.*
951 *Chem. Phys.* 11, 675-688.
- 952 Zanis P., Hadjinicolaou P., Pozzer A., Tyrlis E., Dafka, S., Mihalopoulos N., Lelieveld J., 2014.
953 Summertime free-tropospheric ozone pool over the eastern Mediterranean/Middle East,
954 *Atmos. Chem. Phys.* 14, 115–132.
- 955

956 **FIGURES AND TABLES**
957

958 **Figure Captions**

959 Figure 1. Location of the study area, profiles showing the major orographic patterns and
960 location of three supersites (CSIC, CIEMAT, ISCIII) and the site where vertical profile
961 measurements were carried out (MJDH).

962 Figure 2. Top: Hourly meteorological parameters recorded at El Retiro air quality monitoring
963 station in central Madrid (from 28/06/2016 to 01/08/2016). Middle: Hourly concentrations of
964 O₃ and O_x (O₃+NO₂) recorded at a selection of air quality monitoring station representing the
965 Greater Madrid area, together with those from the remote background station of
966 Campisábalos. Bottom: Hourly NO₂ concentrations recorded at the same sites for the same
967 period. Periods with available AEMET free-soundings of O₃ are bracketed with red
968 (accumulation) or blue (venting) squares. The vertical O₃ and UFP profiling campaign is marked
969 with a green square.

970 Figure 3: Left: Climate Forecast System Reanalysis (CFSR) for the 500 hPa geopotential heights
971 (gpdams) and mean sea level pressure (MSLP) contours (hPa) at 12:00 UTC (obtained from the
972 Climate Forecast System reanalysis, Saha et al., 2014) in July 2016 (Wetterzentrale,
973 <http://www.wetterzentrale.de/>), simultaneous with, Right: AEMET O₃-free soundings at
974 Madrid airport.

975 Figure 4. Variation of meteorological parameters (temperature, relative humidity, solar
976 radiation and wind speed and direction), and levels of NO₂, NO, O₃, PM2.5, PM1, BC and UFP
977 (with lower detection limits of 1, 3 and 7 nm, PN₁, PN₃ and PN₇) measured at Madrid-CSIC,
978 Madrid-CIEMAT and ISCIII, as well as in MJDH-RC from 11 to 14/07/2016.

979 Figure 5. Vertical profiles of levels of O₃, UFP (PN₃), temperature and relative humidity
980 obtained on 14/07/2016 (8:05 to 17:45 UTC). A: Ascending; D: Descending.

981 Figure 6. UFP (PN₃) concentrations for different vertical profiles obtained on 14/07/2016, as
982 well as O₃ and UFP during two periods focusing to evaluate changes produced in a fixed height
983 when reached by the growth of the PBL.

984 Figure 7. Top: Vertical profiles of O₃ levels, and temperature obtained on 12/07/1994 (with
985 free sounding) and 15/07/1993 (with tethered balloons). Data obtained from Plaza et al
986 (1997). Bottom: Vertical profiles of O₃ levels of the free soundings by AEMET at Madrid airport
987 (26.6 km east of MJDH-RC) in 06-07/2017.

988 Figure 8. 11-14/07/2017 profiles of O₃ and UFP (PN₃) grouped by hourly stretches from
989 morning to afternoon.

990 Figure 9. Time evolution of hourly O_x (O₃+NO₂) and O₃ concentrations from 11 to 14/07/2016
991 at selected air quality monitoring sites of the Madrid Basin and an external reference site
992 (Campisábalos), as well as the locations of these monitoring sites.

993 Figure 10. Conceptual model of the venting and accumulation O₃ episodes in the Madrid Air
994 Basin, their associated vertical O₃ profiles and the X (fumigation from upper layers, and flows
995 from free troposphere and stratosphere) and Y (local/regional) contributions to surface O₃
996 concentrations in the accumulation episodes.

997

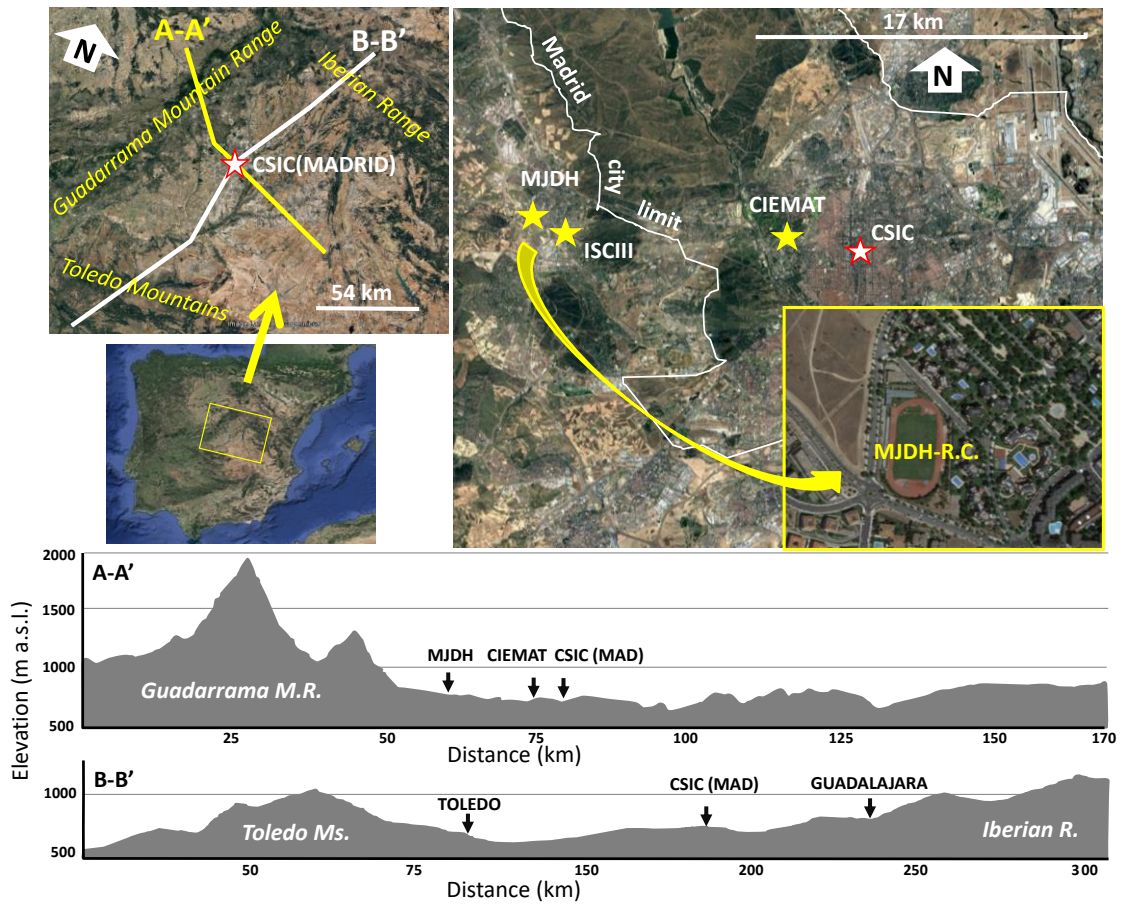


Figure 1

998
999
1000

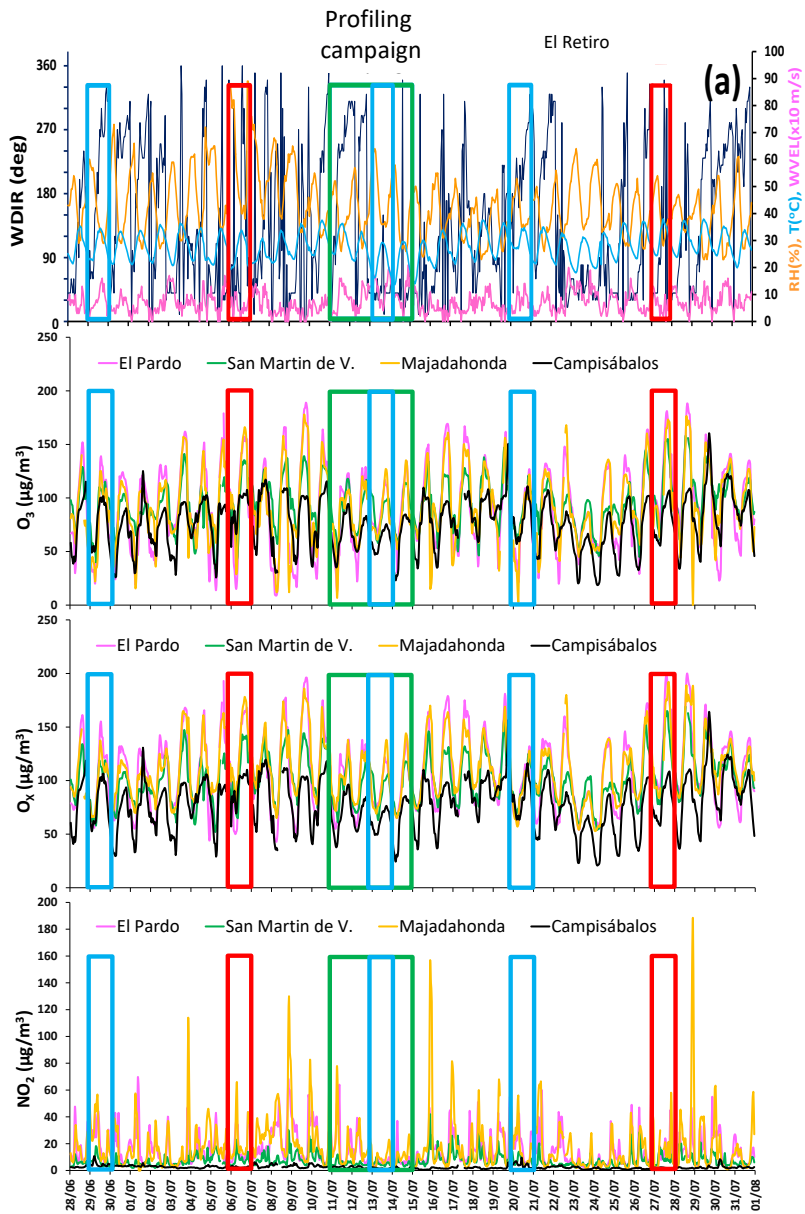
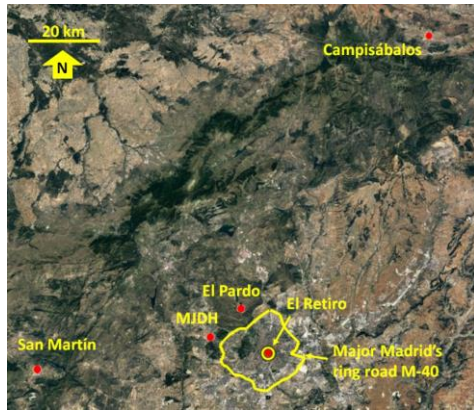


Figure 2

1001
1002
1003

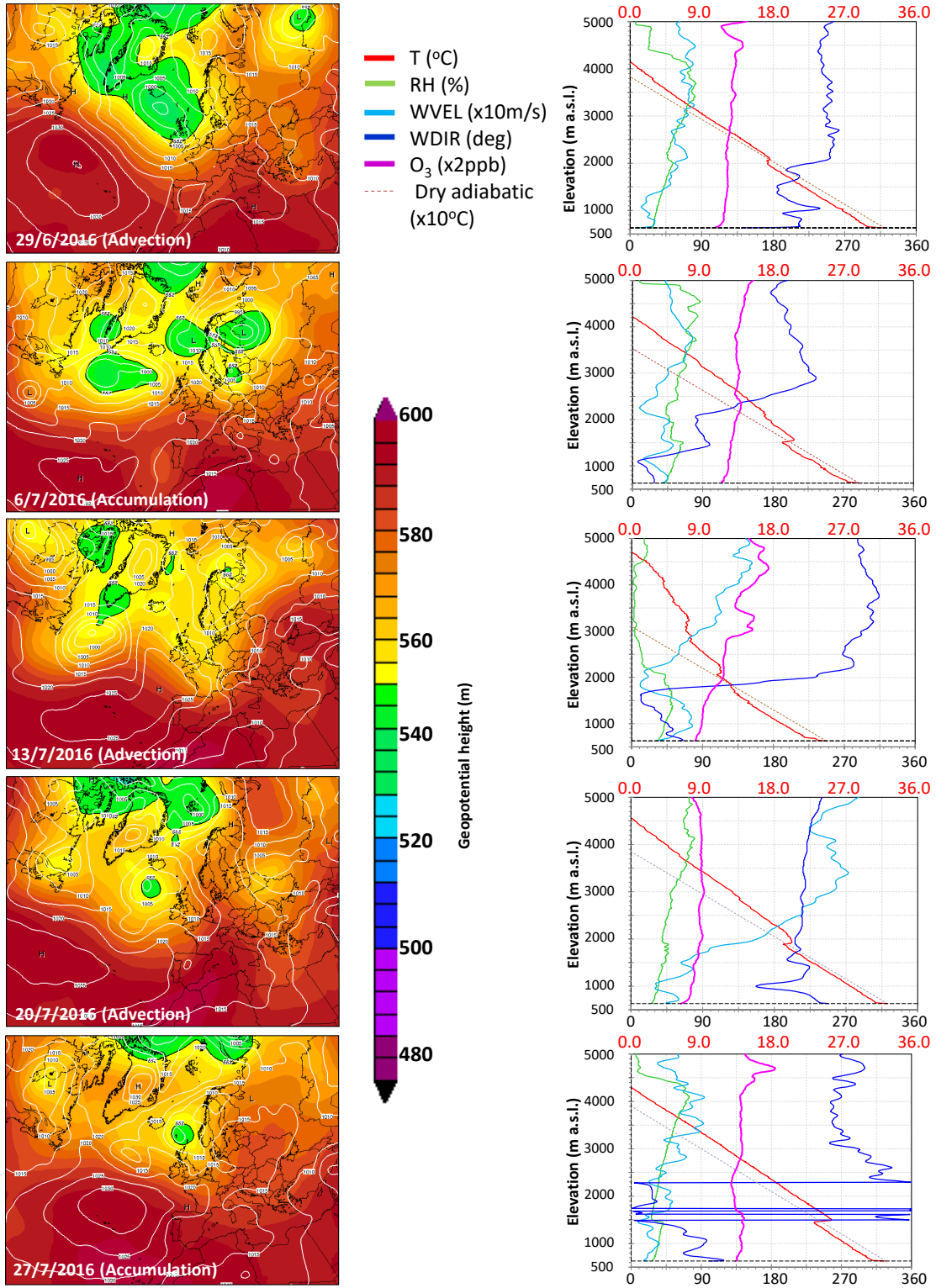
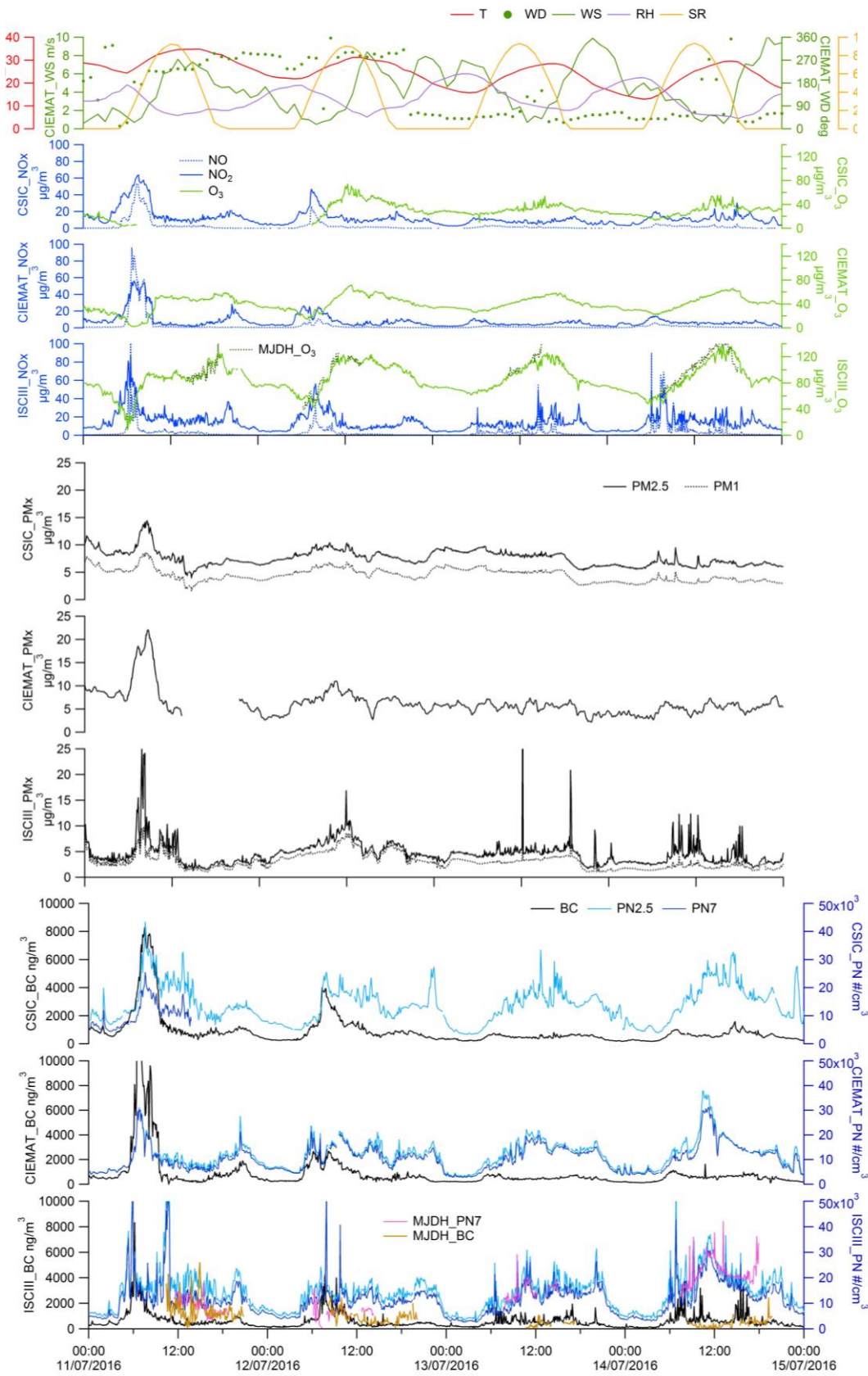


Figure 3

1004
1005
1006

1007



1008
1009
1010

Figure 4

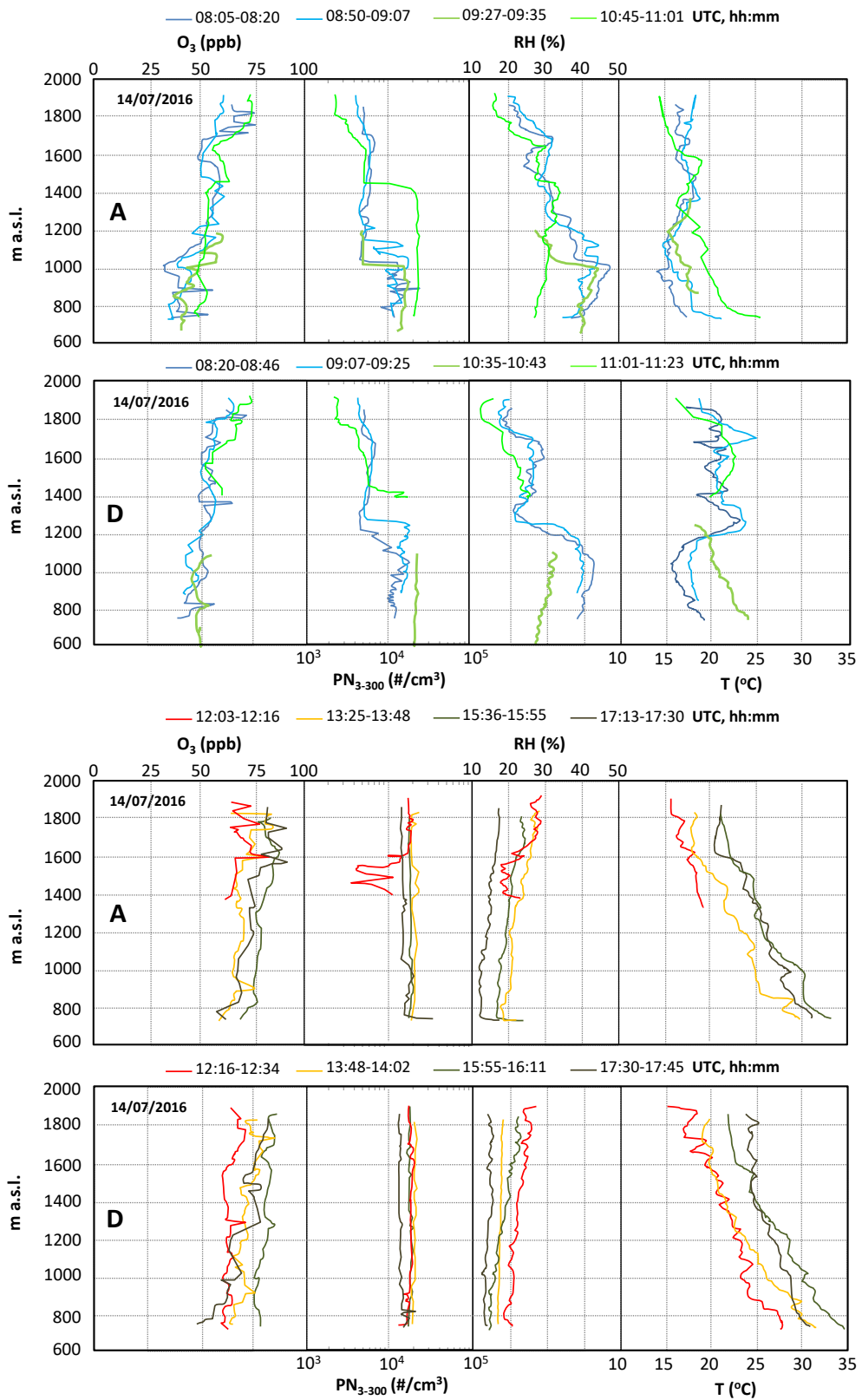
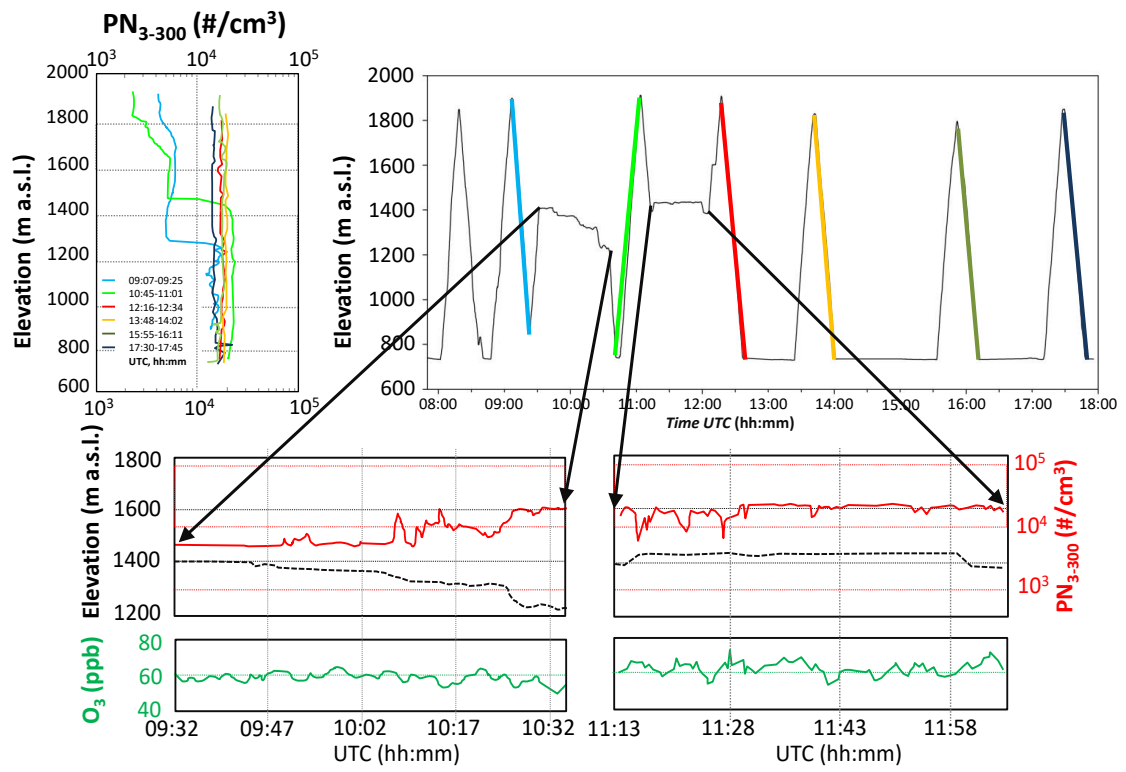


Figure 5

1012
1013
1014



1015
 1016
 1017

Figure 6

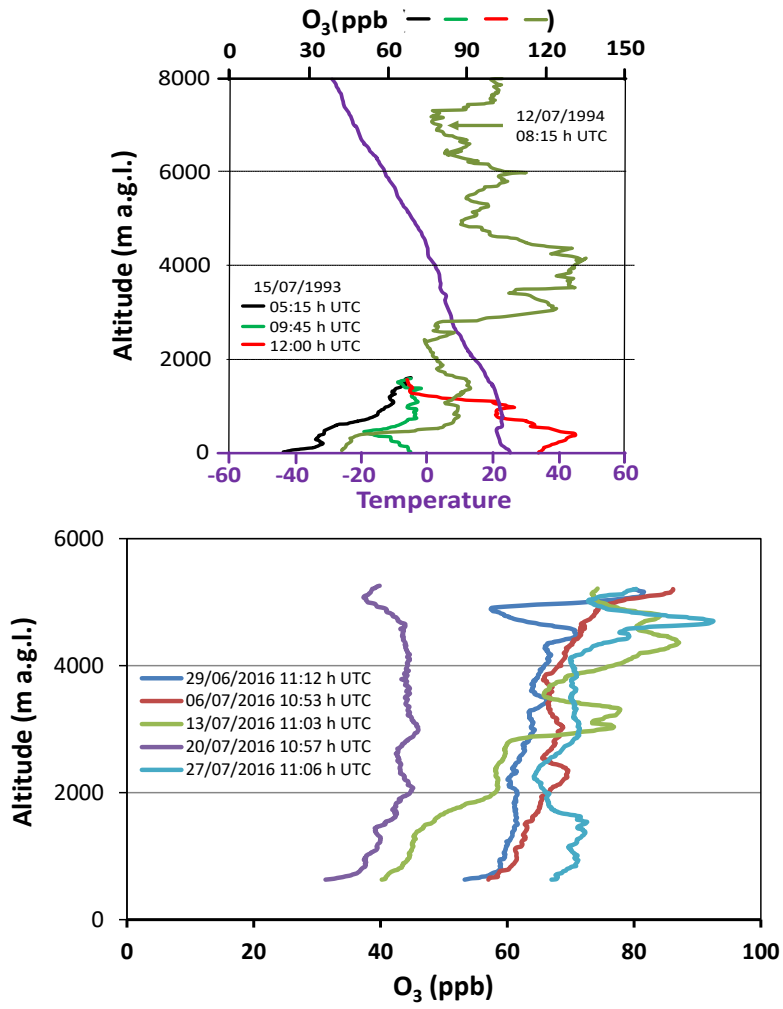


FIGURE 7

1018
1019
1020

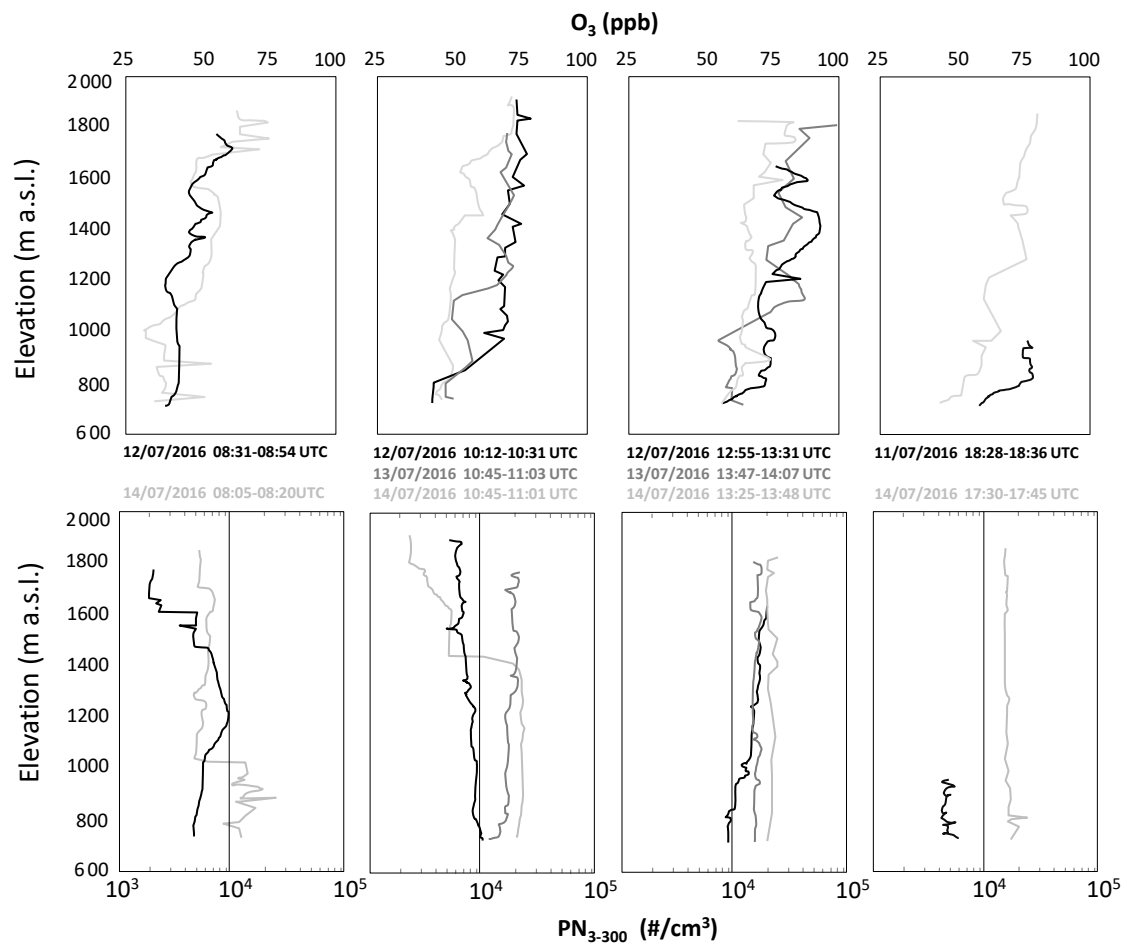


Figure 8

1021
1022
1023
1024

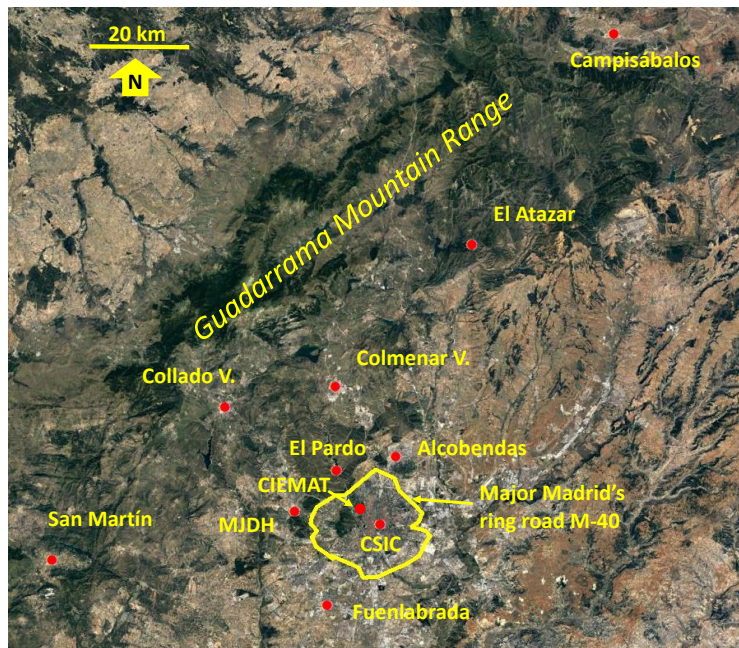
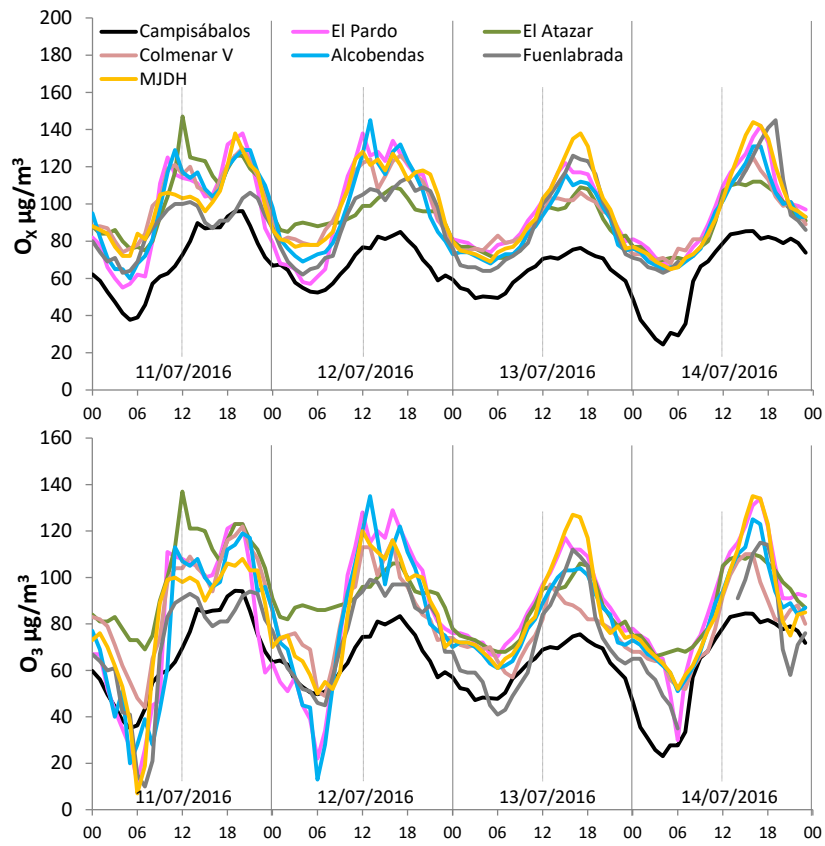
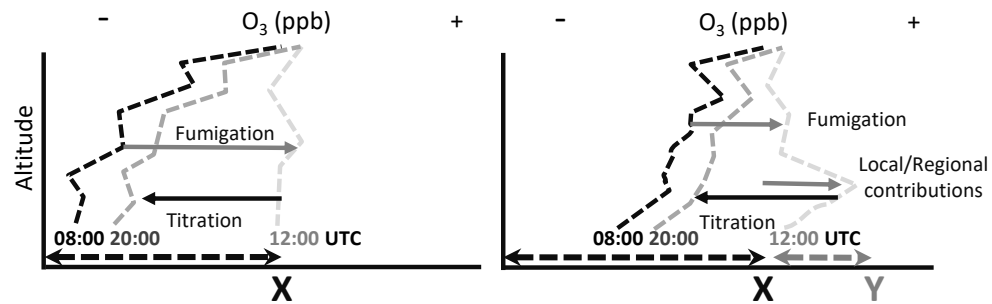


FIGURE 9

1025
1026
1027
1028

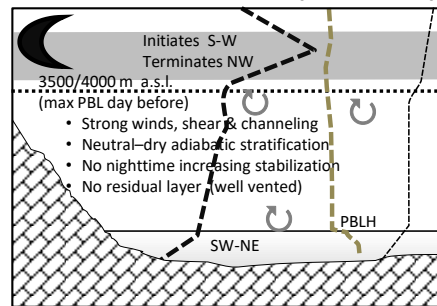


VENTING/TROUGHING (VT EVENT) ACCUMULATING/RIDGING (AR EVENT)

Free troposphere. Strong winds
Occasional high O₃ peaks (free troposphere O₃, stratosphere O₃, long range transport & regional layers)

Low O₃ (mixed, more external)
Intense ventilation, no accumulation from the day before
Mechanical Turbulence

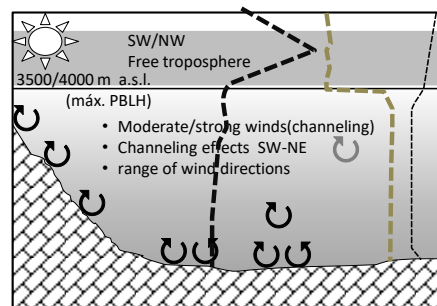
Surface layer, occasionally stably stratified
Low O₃ concentrations, titration
Strong winds SW-NE



Free troposphere. Strong winds
Occasional high O₃ peaks (free troposphere O₃, stratosphere O₃, long range transport & regional layers)

No O₃ accumulation in the PBL
No re-circulatory winds
New O₃ /UFP formation
O₃ fumigation

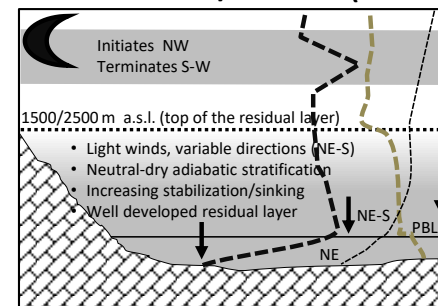
Thicker PBL: > 2000-2500 m a.s.l. at 12:00 UTC
Rapid growing up to 3500/4000 m
Intense mechanical & convective turbulence; Intense convection



Free troposphere. Light winds
Occasional high O₃ peaks (free troposphere O₃, stratosphere O₃, long range transport & regional layers)

Higher O₃ (mixed external + Local)
Low ventilation, re-circulatory winds, accumulation from the day before
No Turbulence

NE'ly jet over stably stratified surface layer
Low O₃ concentrations, titration
Light winds (NE).



Free troposphere. Light winds
Occasional high O₃ peaks (free troposphere O₃, stratosphere O₃, long range transport & regional layers)

O₃ accumulation in the PBL
Re-circulation over the MMA basin
New ozone/UFP formation, O₃ fumigation

Thinner PBL: < 1500 m a.s.l. at 12:00 UTC
Slower deepening to 1500/2500 m
Intense convective turbulence
Additional O₃ formation of local origin
Thermally driven wind veering NE→S →SW
Intense convection

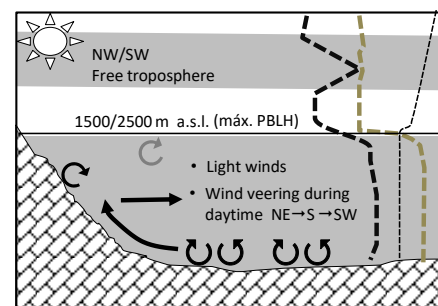


FIGURE 10

1031 **TABLES**

1032 Table 1. Details of the instrumentation used in the three supersites and the platform mounted
 1033 on tethered balloons. BC, black carbon; UFP, ultrafine particles; CPC, condensation particle
 1034 counter; OPC Optical particle counter; MAAP, Multi-angle Absorption Photometre; PTR-ToF-
 1035 MS, Proton Transfer Reaction-Time of Fly-Mass Spectrometer.

Site	Latitude (N)	Longitude (W)	Elevation (m a.s.l.)	Parameter (Device-Model)	Operation period
CSIC	40°26'25"	03°41'17"	713	NO _x (Teledyne API 200EU) O ₃ (2B Technologies 202) UFP>2.5nm (CPC-TSI 3775) BC (Aethalometer-AE33) PM ₁ (OPC-GRIMM 1107)	09-20/07/2016
CIEMAT	40°27'23"	03°43'32"	669	NO _x (THERMO 17i) O ₃ (THERMO 49i) UFP>7nm (CPC-TSI 3772) UFP>2.5nm (CPC-TSI 3776) BC (Aethalometer-AE33) PM _{2.5} (TEOM®) Meteorological tower	04-20/07/2016
ISCIH	40°27'27"	03°51'54"	739	NO _x (THERMO 17i) O ₃ (THERMO 49i) UFP>7nm (CPC-TSI 3783) UFP>2.5nm (CPC-TSI 3776) BC (MAAP-THERMO) PM ₁ (OPC-GRIMM 1108) PTR-ToF-MS (HR 8000, Ionicon)(operating procedures described in SI)	04-20/07/2016
MJDH-RC (vertical profiles)	40°28'30"	03°52'55"	729	UFP>3nm (CPC Hy-CPC) O ₃ (PO3M™ 2B Technologies) Meteorology (temperature., relative humidty, pressure., wind speed and direction)	11-14/07/2016
El Retiro	40°24'55"	3°41 04°	667	Meteorological parameters	04-20/07/2016

1036
1037

1038
1039

Table 2. Vertical measurement profiles obtained during 11-14/07/2016 at Majadahonda (MJDH-RC).

Day	Starting	Final	Number	Maximum
	hour (UTC)	hour (UTC)	of profiles	altitude (m a.g.l.)
11/07/2016	18:30	18:45	2	200
12/07/2012	07:02	07:40	2	850
	08:30	09:10	2	1000
	10:10	10:56	2	1100
	11:55	13:43	2	900
13/07/2008	10:45	11:25	2	1000
	11:25	12:00	2	1000
	13:47	14:29	2	1000
	14:29	15:12	2	1100
14/07/2004	08:03	08:44	2	1150
	08:48	10:37	2	1100
	10:46	12:45	2	1200
	13:22	14:02	2	1100
	15:23	16:13	2	1025
	17:12	17:31	2	1100

1040
1041
1042